Cell Reports

Resource

# The Aging Astrocyte Transcriptome from Multiple Regions of the Mouse Brain

## Graphical Abstract

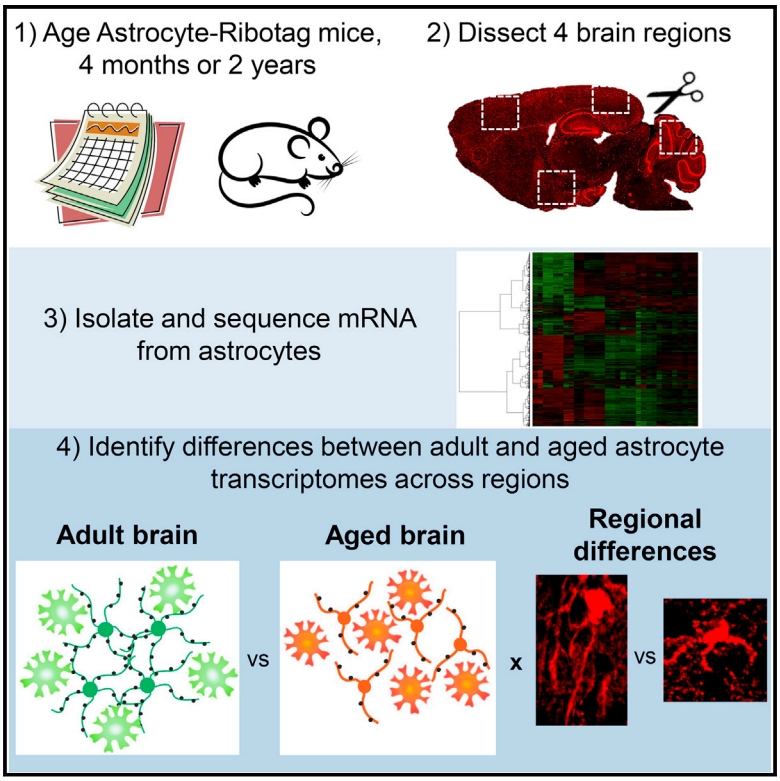



## Authors

Matthew M. Boisvert, Galina A. Erikson, Maxim N. Shokhirev, Nicola J. Allen

## Correspondence

nallen@salk.edu



## In Brief

The aging brain has reduced synapse number and decreased neuronal activity, functions regulated by neighboring astrocytes. Boisvert et al. investigated if aging astrocytes are contributing to these changes and found that aged astrocytes show increased expression of genes for inflammatory and synapse elimination pathways and decreased cholesterol synthesis enzymes.


## Highlights

- Provide astrocyte transcriptome from multiple regions of aged and adult mouse brain
- Astrocytes have a region-dependent aging response, are moderately reactive in aging
- Aged astrocytes increase synapse elimination genes, decrease cholesterol synthesis
- Most astrocyte-enriched genes are differentially expressed between regions

## Data and Software Availability

GSE99791

Boisvert et al., 2018, Cell Reports *22*, 269–285
January 2, 2018 
https://doi.org/10.1016/j.celrep.2017.12.039

CellPress

Cell Reports
Resource



# The Aging Astrocyte Transcriptome from Multiple Regions of the Mouse Brain

Matthew M. Boisvert,[1,3] Galina A. Erikson,[2] Maxim N. Shokhirev,[2] and Nicola J. Allen[1,4,*]
[1]Molecular Neurobiology Laboratory
[2]Razavi Newman Integrative Genomics and Bioinformatics Core
Salk Institute for Biological Studies, 10010 North Torrey Pines Rd., La Jolla, CA 92037, USA
[3]Neurosciences Graduate Program, University of California, San Diego, La Jolla, CA 92093, USA
[4]Lead Contact
*Correspondence: nallen@salk.edu
https://doi.org/10.1016/j.celrep.2017.12.039

## SUMMARY

**Aging brains undergo cognitive decline, associated with decreased neuronal synapse number and function and altered metabolism. Astrocytes regulate neuronal synapse formation and function in development and adulthood, but whether these properties change during aging, contributing to neuronal dysfunction, is unknown. We addressed this by generating aged and adult astrocyte transcriptomes from multiple mouse brain regions. These data provide a comprehensive RNA-seq database of adult and aged astrocyte gene expression, available online as a resource. We identify astrocyte genes altered by aging across brain regions and regionally unique aging changes. Aging astrocytes show minimal alteration of homeostatic and neurotransmission-regulating genes. However, aging astrocytes upregulate genes that eliminate synapses and partially resemble reactive astrocytes. We further identified heterogeneous expression of synapse-regulating genes between astrocytes from different cortical regions. We find that alterations to astrocytes in aging create an environment permissive to synapse elimination and neuronal damage, potentially contributing to aging-associated cognitive decline.**

## INTRODUCTION

In the healthy aging brain, there is a decline in neuronal activity, a loss of synaptic connections, and a decrease in synaptic function (Wang et al., 2011). The magnitudes of these effects vary by brain region (Samson and Barnes, 2013); however, the mechanisms underlying these changes in neuronal and synaptic function are unclear. In the developing and adult brain, non-neuronal glial cells, in particular astrocytes, carry out important functions that regulate synapse number and synaptic communication and support neuronal health and homeostasis (Khakh and Sofroniew, 2015). Whether these astrocytic functions change in the aging brain is not known. Here we explore the hypothesis that decreased neuronal and synaptic function in the aging brain are due to altered properties of astrocytes that negatively affect neurons.

In the forebrain, neuron and astrocyte cell numbers do not significantly change with age, demonstrating that changes in performance are due to altered properties of these cells rather than cell death (Pelvig et al., 2008; Samson and Barnes, 2013). Despite lack of significant cell death, both cortical volume and overall neuronal activity decrease with age, associated with atrophy of neuronal dendrites and an accompanying reduction in dendritic spine number (Pannese, 2011), also evident as a decline in neuronal synapse number. There is a progressive loss of cerebellar Purkinje neurons with age as well as an increase in cerebellar behavioral deficits (Woodruff-Pak et al., 2010). Similarly, extensive stem cell loss is seen in the hypothalamus with age (Zhang et al., 2017), showing that regional differences in aging are present in the brain.

In the developing brain, astrocytes regulate synapse number by secreting synaptogenic signals, such as thrombospondins, hevin, and glypicans, that induce synapse formation (Allen et al., 2012; Christopherson et al., 2005; Kucukdereli et al., 2011) and by eliminating excess synapses by phagocytosis using the receptors Mertk and Megf10 and indirectly by inducing expression of complement cascade components in neurons (Bialas and Stevens, 2013; Chung et al., 2013; Stevens et al., 2007). In the adult brain, astrocytes maintain neuronal and synaptic function, in part through thousands of fine processes that ensheath neuronal synapses (Khakh and Sofroniew, 2015). Functions include recycling neurotransmitters and buffering extracellular potassium to facilitate neuronal transmission (Allen, 2014) and taking up nutrients, including lipids and sugars from the blood, processing them, and delivering them to neurons for energy (van Deijk et al., 2017). Therefore, astrocytes play essential roles in regulating synaptic connectivity and function during development and in the adult.

To find out whether astrocyte function is altered in the aging brain and contributes to decreased neuronal and synaptic function, we took a transcriptomic approach. We isolated mRNA from astrocytes from multiple regions of the adult (4 months) and aging (2 years) mouse brain, allowing us to determine whether astrocyte gene expression changes with age are global or show regional specificity, which is particularly important because heterogeneity exists between astrocytes from different

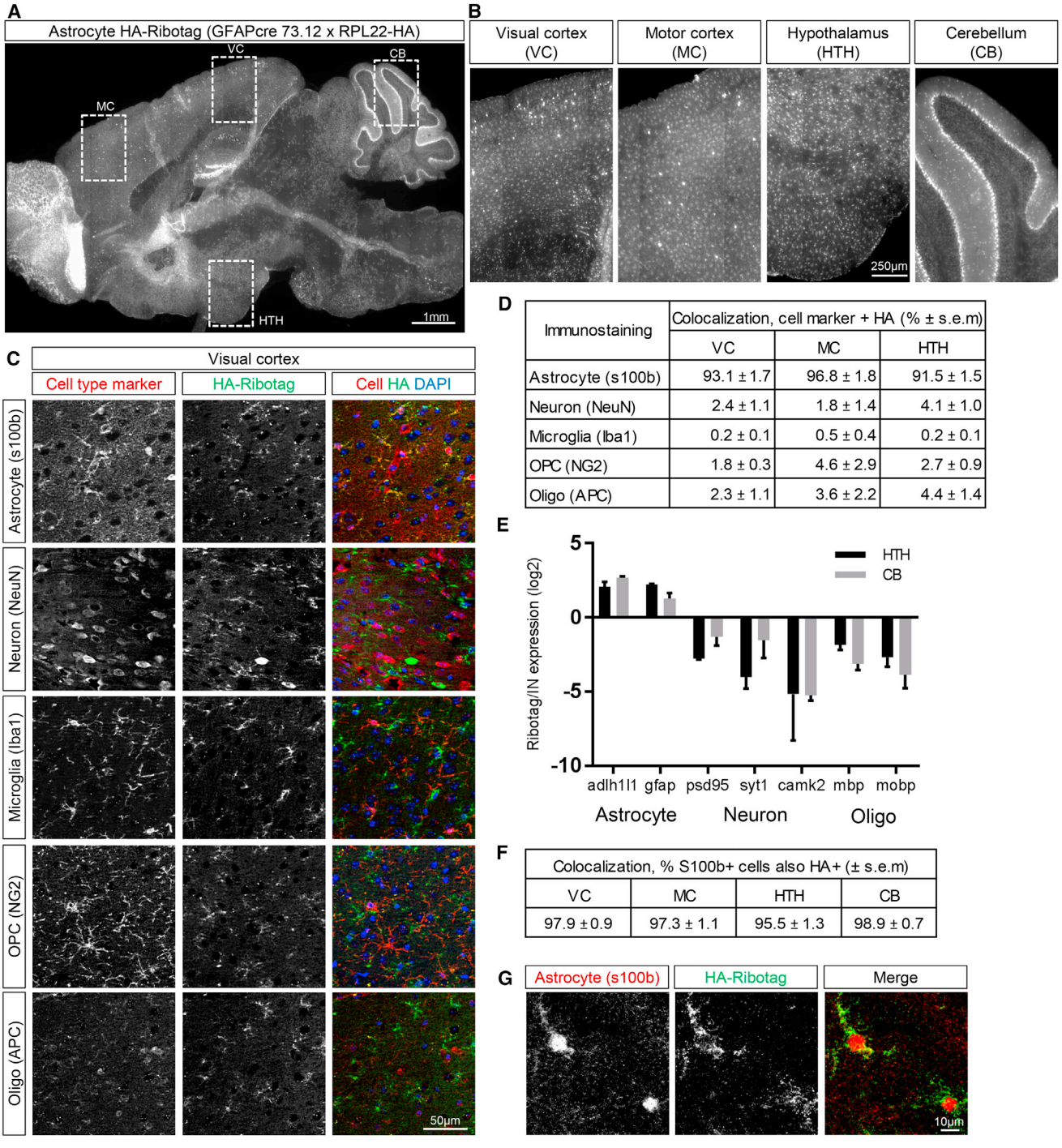


| Immunostaining | Colocalization, cell marker + HA (% ± s.e.m) | | |
|---|---|---|---|
| | VC | MC | HTH |
| Astrocyte (s100b) | 93.1 ± 1.7 | 96.8 ± 1.8 | 91.5 ± 1.5 |
| Neuron (NeuN) | 2.4 ± 1.1 | 1.8 ± 1.4 | 4.1 ± 1.0 |
| Microglia (Iba1) | 0.2 ± 0.1 | 0.5 ± 0.4 | 0.2 ± 0.1 |
| OPC (NG2) | 1.8 ± 0.3 | 4.6 ± 2.9 | 2.7 ± 0.9 |
| Oligo (APC) | 2.3 ± 1.1 | 3.6 ± 2.2 | 4.4 ± 1.4 |

| Colocalization, % S100b+ cells also HA+ (± s.e.m) | | | |
|---|---|---|---|
| VC | MC | HTH | CB |
| 97.9 ± 0.9 | 97.3 ± 1.1 | 95.5 ± 1.3 | 98.9 ± 0.7 |

(legend on next page)

brain areas (Chai et al., 2017). To specifically isolate astrocyte mRNA, we used the ribotag technique to genetically tag ribosomes in astrocytes (Sanz et al., 2009), restricting analysis to astrocytes and enabling purification of astrocyte-associated mRNA throughout the entire cell, including in the fine processes. We used RNA sequencing to identify and quantify astrocyte mRNA, providing unbiased identification of gene expression changes. Prior work has inferred astrocyte changes in aging from whole-brain data (Cribbs et al., 2012; Soreq et al., 2017) or used less physiological isolation methods, such as culturing astrocytes (Bellaver et al., 2017; Jiang and Cadenas, 2014), which alters gene expression, or fluorescence-activated cell sorting (FACS) (Orre et al., 2014), which allows only mRNA from the cell body to be isolated, or used a microarray to identify genes (Orre et al., 2014).

This approach has generated a comprehensive dataset of astrocyte gene expression from multiple regions of the adult and aging brain. We have made this dataset freely available as a resource by generation of a website, allowing anyone to investigate how astrocytes change with age. We used these data to determine key changes to astrocytes in the aging brain and to find out whether these changes could negatively affect synaptic and neuronal function. We further interrogated astrocyte differences between cortical regions as well as between astrocytes from 3 distinct brain regions, identifying differential expression of synapse-regulating genes.

## RESULTS

### Generation of an Astrocyte-Ribotag Mouse Model for Purification of Astrocyte-Enriched mRNA from the Adult and Aging Brain

To isolate astrocyte-enriched mRNA, we employed a genetic strategy to affinity-tag ribosomal subunits in astrocytes, referred to as astrocyte-ribotag. We crossed floxed-*Rpl22*-HA mice (a cre-dependent hemagglutinin [HA] tag on ribosomal subunit 22) (Sanz et al., 2009) to a *Gfap*-cre mouse line (expression of cre recombinase under the *Gfap* promoter to restrict expression to astrocytes) (Garcia et al., 2004). In cells expressing cre recombinase, an HA-tagged ribosomal subunit is produced, which allows for affinity purification of HA-tagged ribosomes and associated mRNA using an antibody against HA (Figure 1H; Chai et al., 2017; Sanz et al., 2009). Immunostaining against the HA tag demonstrated widespread expression of HA-tagged ribosomes in most brain regions at 4 months, including the cortex, cerebellum, and subcortical areas (Figure 1A). Based on this, we focused our studies on astrocyte aging in the visual cortex (VC), motor cortex (MC), cerebellum (CB) and hypothalamus (HTH) (Figures 1A and 1B).

To determine whether astrocytes are the major cell type expressing HA-tagged ribosomes, we immunostained brain sections for HA along with antibodies against cell-specific markers (astrocytes, S100b; neurons, neuronal nuclear antigen [NeuN]; oligodendrocyte precursor cells, NG2; oligodendrocytes, APC; microglia, Iba1; Figure 1C, VC; Figures S1 and S2A, other regions). We found a 92%–97% overlap between HA and the astrocyte marker S100b in the VC, MC, and HTH (Figure 1D), with the rest of the HA-positive cells being neurons (2%–4%) or of the oligodendrocyte lineage (2%–4%). In the HTH, a subset of ependymal cells lining the third ventricle expressed HA ($\alpha$ tanycytes, which derive from the GFAP lineage and share astrocyte properties (Goodman and Hajihosseini, 2015; Figures S2B and S2C). The high density of immunostaining in the CB made quantification challenging, so we used qRT-PCR to determine cell type enrichment. In both the CB and HTH (as a comparison), mRNA for astrocyte markers is strongly enriched in the pull-down compared with total mRNA from all cells (input), and expression of neuronal and oligodendrocyte lineage genes is decreased (Figure 1E). The majority of astrocytes in each brain region also express HA-tagged ribosomes (96%–99% of S100b cells are HA-positive; Figure 1F). We further confirmed that HA-tagged ribosomes are present throughout the astrocyte, including distal processes where local translation occurs (Figure 1G; Sakers et al., 2017).

### Purification and Sequencing of Astrocyte-Enriched mRNA from Multiple Brain Regions of Adult and Aging Mice

To find out whether astrocyte gene expression is altered in the aging brain, we isolated astrocyte-enriched mRNA from multiple brain regions, as validated in Figure 1—the VC, MC, HTH, and CB. We looked at 2 time points: 4 months (adult), when developmental changes to astrocyte gene expression have ceased, and 2 years (aging), before age-dependent pathology develops. We used RNA sequencing (RNA-seq) to identify and quantify the mRNA. For each time point and brain region, we sequenced 3 astrocyte-ribotag samples from separate mice and an input sample (mRNA from all cells) to provide a reference for

**Figure 1. Characterization of the Astrocyte-Ribotag Mouse Model**

(A) Sagittal brain section from 4-month-old astrocyte-ribotag mouse immunostained for HA to visualize ribosomes; image is a mosaic of tile images acquired at 10x.

(B) Zoomed-in images from (A), regions of HA-tagged ribosome purification (VC, MC, HTH, CB); images are cropped from the mosaic tile image.

(C) Immunostaining for HA and cell-specific markers in VC to determine cell-type expression of HA-tagged ribosomes. Images cropped from a larger mosaic of tiles acquired at 20x.

(D) Quantification of cell-specific staining shows majority of HA-tagged ribosomes are in astrocytes. n = 3 × 4 month mice/brain region.

(E) qRT-PCR from HTH and CB astrocyte-ribotag-isolated mRNA shows enrichment for astrocyte mRNAs over other cell types, compared to total (input) mRNA. n = 3 × 2 year mice/brain region; graph mean ± SEM.

(F) Quantification of S100b positive cells that are also HA positive; n = 3 × 4 month mice/brain region.

(G) Immunostaining for HA and S100b shows ribosomes present throughout astrocyte processes in VC.

(H) Schematic of the experimental paradigm—purification of astrocyte-enriched mRNA from multiple brain regions of adult (4-month-old) and aging (2-year-old) mice, followed by RNA-seq and analysis.

See also Figures S1 and S2.

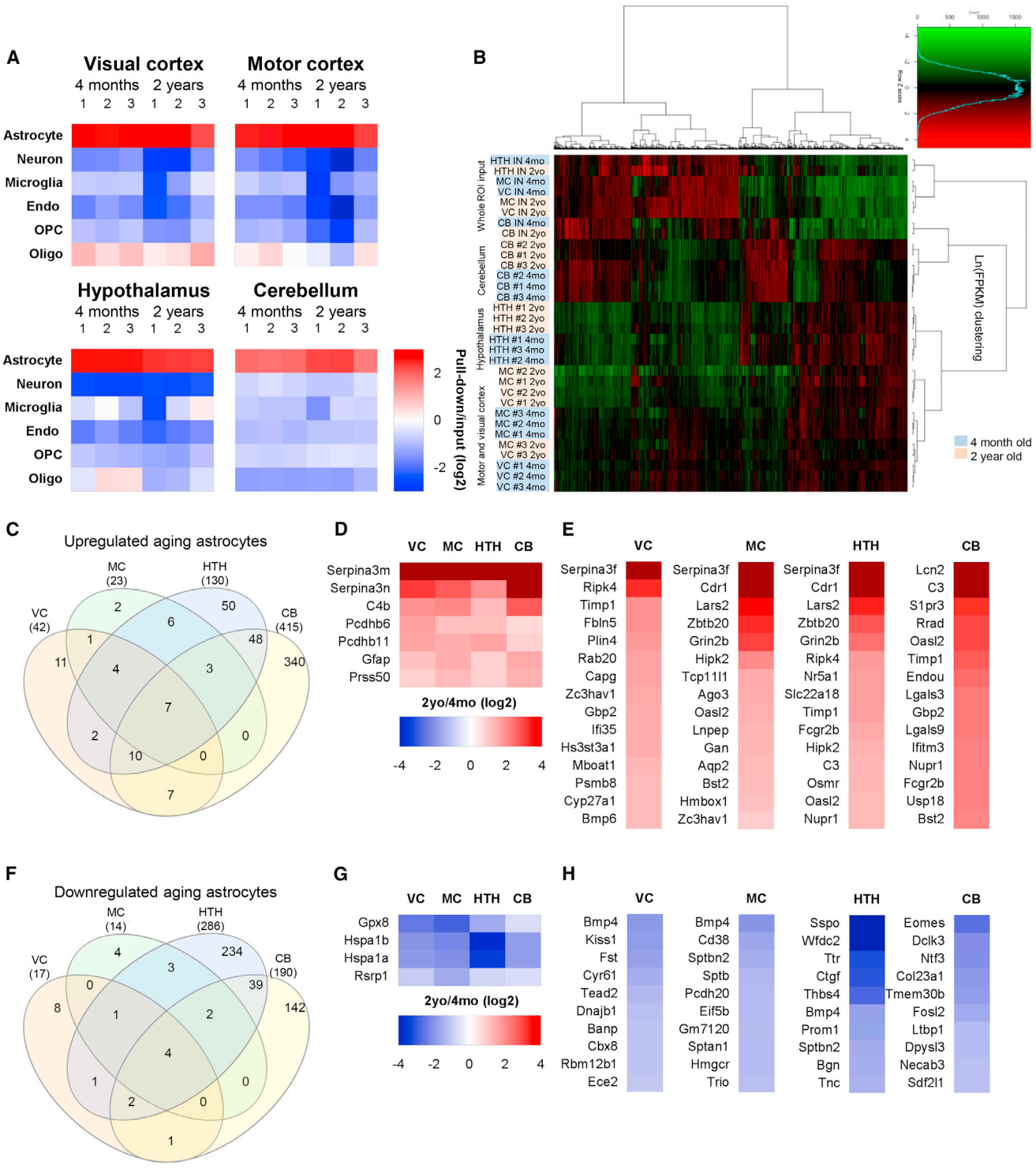


**Figure 2. Purification and RNA-Seq of Astrocyte-Enriched mRNA Identifies Differentially Expressed Genes between Adult and Aging Astrocytes**

(A) Analysis of RNA-seq data for cell-specific mRNA demonstrates enrichment for astrocytes over other cell types in the pull-down (astrocyte mRNA) compared with input (total mRNA) (see Table S1 for the gene list).

(B) Clustering analysis of the top 4,401 expressed genes shows that astrocyte-ribotag pull-down samples cluster away from input mRNA; samples cluster by region of isolation and, within region, by age. n = 3 mice for each brain region and age (astrocyte samples). See Table S2 for FPKM for all genes.

(C) Venn diagram showing overlap of genes upregulated in astrocytes from 4 different brain regions between 4 months and 2 years.

*(legend continued on next page)*

determining astrocyte enrichment (Figure 1H). To quantify astrocyte enrichment, we developed a list of cell-specific markers from published RNA-seq and microarray data of purified cortical cell types from the developing brain (see Table S1 for a list; Cahoy et al., 2008; Zhang et al., 2014). Comparison of astrocyte-ribotag mRNA levels with the input shows a 6-fold enrichment for astrocyte genes in all brain regions at both ages, along with a depletion of neuronal and microglial genes and decreased levels of endothelial and oligodendrocyte lineage genes (Figure 2A). We further compared the cerebellar data with cerebellar cell-type-specific microarray data (Doyle et al., 2008), finding a 3- to 5-fold enrichment for astrocyte and Bergmann glia genes and a depletion of other cell types (Figure S1C).

Having validated that astrocyte-ribotag samples are enriched for astrocyte mRNA, we performed a clustering analysis on all samples using the top expressed genes. This showed that biological replicates from the same brain region group together and that input samples (all cells) segregate away from astrocytes. Astrocytes from each cortical region are more similar to each other than astrocytes from non-cortical regions, and, within a brain region, the majority of samples cluster by age at isolation (Figure 2B). This shows that astrocytes from different brain regions have distinct gene expression profiles and that these profiles change with age. This now provides a dataset we can use to find out how astrocyte gene expression changes in the aging brain (Table S2), available online as a resource at http://igc1.salk.edu:3838/astrocyte_aging_transcriptome/.

## Identification of Gene Expression Changes Between Adult and Aging Astrocytes from Multiple Brain Regions

We first determined the number of genes that are significantly upregulated or downregulated ($p < 0.05$ adjusted for multiple comparisons) in astrocytes by aging in each individual brain region. We found the least changes in cortical astrocytes (< 100 genes) and the most in the HTH and cerebellum (> 500) (Table S3). We then filtered for genes that are significantly altered (adjusted $p < 0.05$), expressed at an appreciable level (fragments per kilobase of transcript per million mapped reads [FPKM] > 1) and are astrocyte-expressed (pull-down/input > 0.75) (Experimental Procedures). This identified 42 upregulated genes in the VC, 23 in the MC, 130 in the HTH, and 415 in the CB (Figure 2C; Table S4; top 15 upregulated genes/region, Figure 2E). To identify core aging-upregulated genes, we looked for overlap in gene expression changes between all brain regions and identified 7 genes (Figure 2D), including markers of reactive astrocytes, *Gfap* and *Serpina3n* (Zamanian et al., 2012), and a component of the complement cascade involved in synapse elimination, *C4b* (Sekar et al., 2016). β-Protocadherins are upregulated in all astrocytes by aging, and although little is known about their function, the related γ-protocadherins have important roles in developmental synapse formation (Peek et al., 2017). To determine whether any of the upregulated genes are region-specific, we generated lists of genes that are uniquely upregulated in astrocytes in one brain region or showed overlap with 1 or 2 other regions (Table S4). This showed a specific increase in *Bmp6* in VC astrocytes with age, along with the negative synaptic regulator *Sparc* (see below). The CB has unique pro-inflammatory changes with age, with *caspase-1* and *-12*, the chemokine *Cxcl5*, and the key inflammasome receptors *Tlr2* and *4* all going up.

We applied the same filtering criteria to identify genes that are downregulated in aging astrocytes. This identified 17 genes in the VC, 14 in the MC, 286 in the HTH, and 190 in the CB (Figure 2F; Table S4; top 10 decreased genes/region, Figure 2H). There are 4 core genes significantly downregulated in astrocytes in all brain regions, 2 of which are heat shock proteins (Figure 2G), protective molecular chaperones that prevent protein damage (Bobkova et al., 2015). We next generated lists of genes that are uniquely downregulated in astrocytes in one brain region or showed overlap with 1 or 2 other regions (Table S4). *Bmp4* is downregulated with aging in the VC, MC, and HTH but not the CB, appearing to oppose the increase in *Bmp6* observed with age in the VC. In the HTH, the extracellular matrix factor *Tnc*, associated with the astrocyte injury response, goes down, as do multiple amino acid transporters. These data identify core changes that are common to all astrocytes in the aging brain as well as unique region-dependent aging responses.

## Validation of Aging Astrocyte Gene Expression Changes by *In Situ* Hybridization

We next validated the ability of RNA-seq to reliably detect mRNA changes in aging astrocytes using RNAscope *in situ* hybridization in 4-month- and 2-year-old VCs of wild-type mice. We examined upregulated genes (*C4* and *Sparc*), a downregulated gene (*Hspa1b*), and a gene that did not change with age (*Gpc5*) in the RNA-seq analysis. In the aging brain, we detected high levels of autofluorescence from lipofuscin granules, an accumulation of lipids characteristic of aging brain tissue (Gray and Woulfe, 2005). The lipofuscin colocalizes with neuronal and microglial markers in the cortex and HTH, with little found in astrocytes (Figures S3C and S3D), whereas extensive lipofuscin is seen in Bergmann glia in the CB (Figure S3D). To allow image analysis, the lipofuscin signal was removed by masking (example images in Figures S3A and S3B; Experimental Procedures). We quantified the total signal intensity of the probe and detected a similar fold change in mRNA as in the RNA-seq—an increase in *C4* and *Sparc* with age, no change in *Gpc5*, and a decrease in *Hspa1b* (Figures 3A–3H; Figures S4A–S4D). *C4* mRNA was also increased in the aging HTH, matching the RNA-seq (Figures 3A and 3B; Figure S4E). As an alternative approach, we quantified the total volume of the mRNA signal, which yielded the same fold change in mRNA level (Figure S4F).

(D) Heatmap of genes that are significantly upregulated in astrocytes by aging in all regions.
(E) Heatmaps of top 15 genes upregulated in astrocytes in each brain region by aging (excluding those in D; see Tables S3 and S4 for a full list).
(F) Venn diagram of genes downregulated in astrocytes from 4 different brain regions between 4 months and 2 years.
(G) Heatmap of genes that are significantly downregulated in astrocytes by aging in all regions.
(H) Heatmaps of the top 10 genes downregulated in astrocytes in each brain region by aging (excluding those in G; see Tables S3 and S4 for a full list).
All heatmaps presented as fold change 2 years/4 months (log2). See also Figure S1 and Tables S1, S2, S3, and S4.

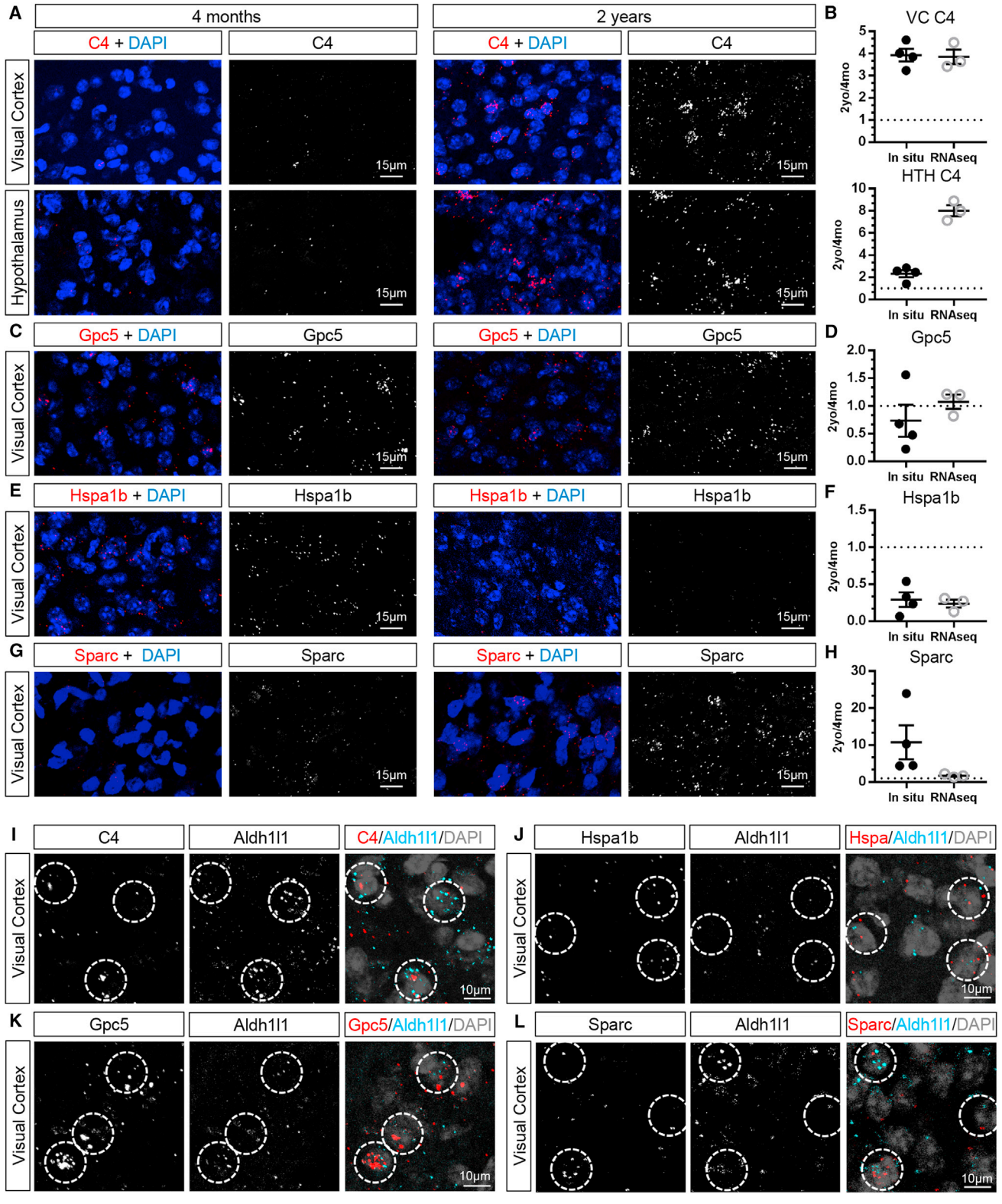


**Figure 3. Validation of Aging-Induced Changes in Astrocyte Gene Expression by *In Situ* Hybridization**

(A, C, E, and G) *In situ* hybridization to detect mRNA for candidate genes in 4-month-old (left) and 2-year-old (right) mouse brains, with lipofuscin subtracted for clarity (as in Figure S3). Shown are *in situ* hybridization for a gene upregulated in astrocytes by aging in the VC and HTH, *C4* (A); unchanged in the VC, *Gpc5* (C); downregulated in the VC, *Hspa1b* (E); and upregulated in the VC, *Sparc* (G). For whole-region images encompassing the area analyzed, see Figure S4.

*(legend continued on next page)*

We next validated astrocyte expression of target genes by probing for the gene of interest along with the astrocyte marker *Aldh1l1*, showing overlap between *Aldh1l1* and all of the genes of interest (*C4*, *Sparc*, *Gpc5*, and *Hspa1b*) (Figures 3I–3L). As an additional validation, we normalized the target probe signal to the *Aldh1l1* signal as an internal control and again found the same trends in altered gene expression with age (Figure S4G). Taken together, this shows that astrocyte-ribotag RNA-seq reliably detects upregulated, downregulated, and unchanging gene expression in aging astrocytes.

## Aging Astrocytes Show Altered Expression of Synapse-Regulating Genes

Our hypothesis is that changes in astrocyte properties, reflected as changes in gene expression, are contributing to impaired synaptic and neuronal function in the aging brain. We therefore asked whether genes expressed by astrocytes that regulate synapses during development are altered in aging and contribute to synapse loss (Figure 4A). We examined known synapse-inducing genes, thrombospondins (Thbs) and *Sparcl1* (Hevin) (Christopherson et al., 2005; Kucukdereli et al., 2011), as well as astrocytic regulators of synaptic strength, *Glypican 4* and *6* (Allen et al., 2012). Glypican and hevin expression are not altered in any brain region between 4 months and 2 years, and *Thbs1, 2*, and *4* are not altered in the aging cortex. There is a significant decrease in *Thbs4* in the aging HTH (Figure 4B), whereas, in the CB, there is a significant decrease in *Thbs1* and an increase in *Thbs2* with age (Figure 4B). *Sparc* inhibits synapse function by blocking synapse formation and decreasing synaptic $\alpha$-amino-3-hydroxy-5-methyl-4-isoxazolepropionic acid (AMPA) receptors (Allen, 2014). There is a significant 2-fold increase in *Sparc* in the aging VC, confirmed by *in situ* hybridization (Figure 3G), with the same trend in the MC, suggesting that, in the aging cortex, increased production of *Sparc* may inhibit synaptic function and block new synapse formation (Figure 4B).

Astrocytes regulate synapse elimination during development by secreting transforming growth factor $\beta$ (TGF-$\beta$), which induces components of the complement cascade in neurons (*C1q*), and by direct phagocytosis of synapses using *Mertk* and *Megf10* (Bialas and Stevens, 2013; Chung et al., 2013; Stevens et al., 2007). There is no change in *TGF-$\beta$1–3* expression in aging astrocytes, except for a significant 2-fold increase in *TGF-$\beta$2* in cerebellar astrocytes (Figure 4B). Interestingly, *C3*, a part of the classical complement cascade required for synapse elimination (Stevens et al., 2007), is strongly upregulated in aging astrocytes in all brain regions examined, as are other members of the complement cascade (see below) (Figure 4F). Expression of *Megf10* and *Mertk* is not altered, suggesting that there is no increase in direct phagocytosis of synapses by aging astrocytes (Figure 4B). Taken together, these data support an active role for astrocytes in eliminating synapses in the aging brain by upregulating expression of genes known to be involved in synapse elimination, with limited alterations in the expression of genes that induce synapse formation.

## Astrocyte Homeostasis Genes Are Largely Unchanged with Aging

We next asked whether genes considered markers of astrocytes are altered by aging, including the cytoskeletal markers *Gfap* and vimentin, the cytosolic markers *S100b*, *Aldoc*, and *Aldh1l1*, the lipoprotein *Apoe*, and the water channel *Aqp4* (Figure 4C). Of these, only *Gfap* is significantly altered in astrocytes in all brain regions by aging, with a 2- to 3-fold increase in expression (Figure 4D). *Gfap* is a known marker of reactive astrocytes, and this is explored more in Figure 5 (Zamanian et al., 2012). In the adult brain, astrocytes regulate synaptic transmission and neuronal homeostasis through a number of pathways (Figure 4C; Allen, 2014). Astrocyte expression of Kir4.1 (*Kcjn10*), the major channel involved in potassium uptake, is unchanged by aging. The glutamate uptake transporters Glt1 and glutamate aspartate transporter (GLAST) (*Slc1a2* and *Slc1a3*), the glutamate-metabolizing enzyme glutamine synthetase (*Glul*), and the $\gamma$-aminobutyric acid (GABA) transporter GAT3 (*Slc6a11*) are not significantly altered by aging (Figure 4D). Astrocytes express numerous channels and neurotransmitter receptors and can respond to activation of receptors with increases in intracellular calcium and release of neuromodulators (Figure 4C; Khakh and Sofroniew, 2015). Examination of genes related to these functions, including connexins, metabotropic glutamate and GABA receptors, calcium channels, and ATP receptors, revealed no significant change in expression with aging, except for a decrease in CB *Gabbr2* (Figure 4D). Components of the lactate shuttle (e.g., *Ldha* and *Mct1*), which supply neurons with lactate for metabolism, are also unaltered in aging astrocytes, as is the transcription factor regulating lipid synthesis, sterol regulatory element-binding proteins (*Srebf1*) (Figure 4D). Therefore, the expression of genes related to major functions of astrocytes in relation to synaptic transmission and neuronal homeostasis is not altered in the aging brain, demonstrating that there is not a general loss of astrocyte support of neurons with age.

## Pathway Analysis Identified that Aging Astrocytes Increase Expression of Immune Pathways and Decrease Cholesterol Synthesis

As an unbiased approach to identify alterations in aging astrocytes, we carried out a pathway analysis of the top changed genes in each brain region (Table S5). Fitting with the pattern of individual gene expression changes, the majority of pathways altered in aging were in the CB and HTH rather than in the cortex. A pathway downregulated in aging astrocytes in multiple brain regions is the cholesterol synthesis pathway (Figure 4E), with the major rate-limiting enzyme, *Hmgcr*, significantly decreased

(B, D, F, and H) Quantification of fold change in mRNA expression detected by *in situ* hybridization between 2 years and 4 months compared with fold change detected by RNA-seq, showing similar fold change (B: C4; D: Gpc5; F: Hspa1b; H: Sparc). Data are presented as a scatterplot of individual points with mean ± SEM. *In situ*, n = 4 4-month-old and 4 2-year-old mice; RNA-seq, n = 3 4-month-old and 3 2-year-old mice.

(I–L) Double *in situ* hybridization with the astrocyte marker *Aldh1l1* and *C4* (I), *Gpc5* (K), and *Sparc* (L) in 2-year-old VC and *Hspa1b* (J) in 4-month-old VC. Circles mark astrocytes expressing the target probe and Aldh1l1.

See also Figures S3 and S4.

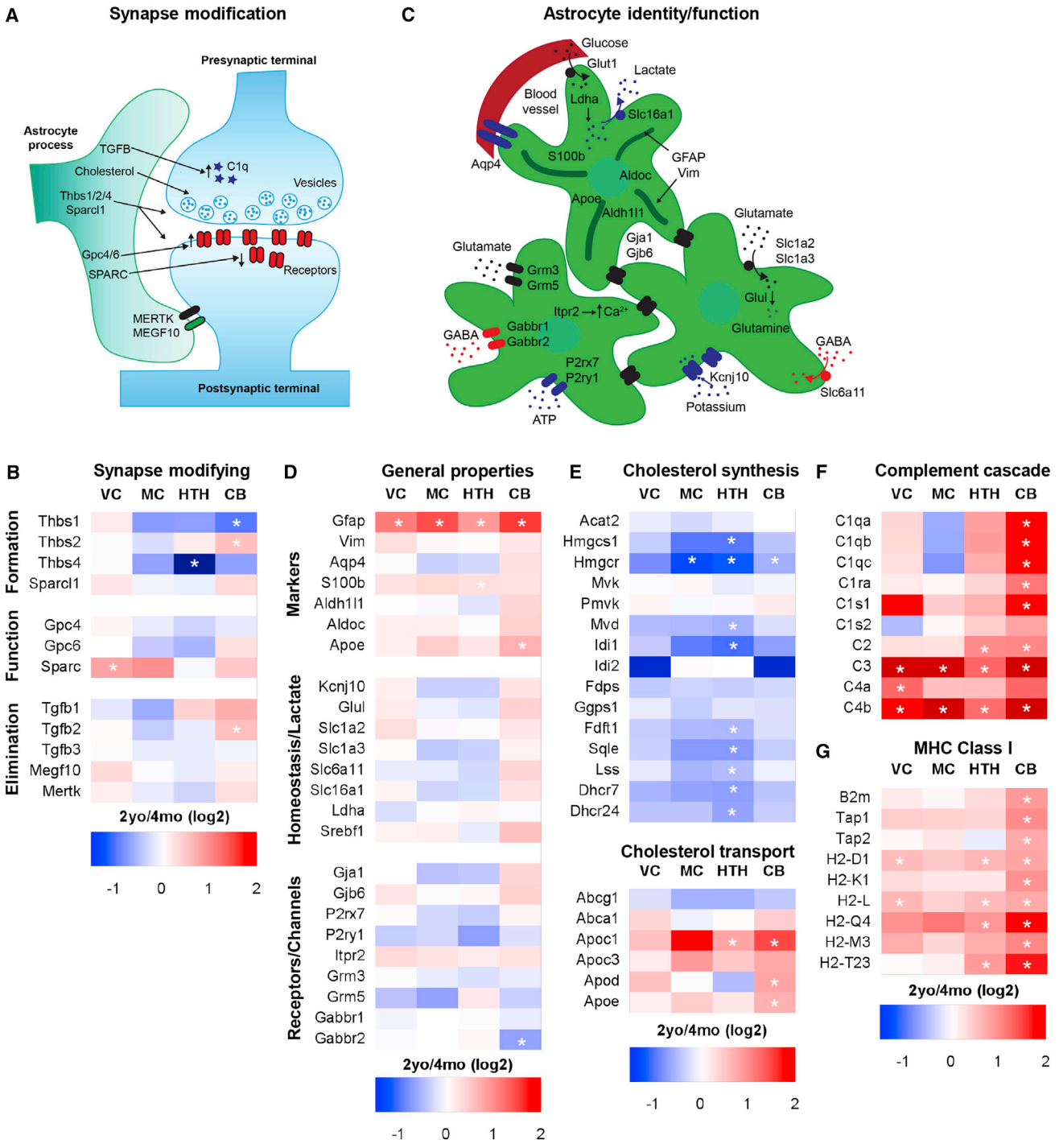


**Figure 4. Astrocyte Marker and Synapse-Modifying Gene Expression in the Aging Brain**

(A and B) Schematic of astrocyte-expressed genes that regulate neuronal synapse formation, function, and elimination (A), with the corresponding heatmap (B) demonstrating region-specific increased expression of genes that inhibit synaptic function and eliminate synapses.

(C and D) Schematic of genes important for astrocyte identity and function: astrocyte markers and metabolism (top astrocyte), homeostatic functions (right astrocyte), and neurotransmitter receptors (left astrocyte) (C), with the corresponding heatmap (D) showing minimal changes in aging.

(E) Enzymes in the cholesterol synthesis pathway are downregulated in aging astrocytes, whereas cholesterol-transporting proteins are upregulated.

(F and G) Immune/antigenic response pathways implicated in synapse elimination, the complement cascade (F), and MHC (G), are upregulated in aging astrocytes. All heatmaps are presented as 2-year/4-month (log2) fold change for each brain region. *, significantly altered between 2-year and 4-month astrocytes. See also Table S5.

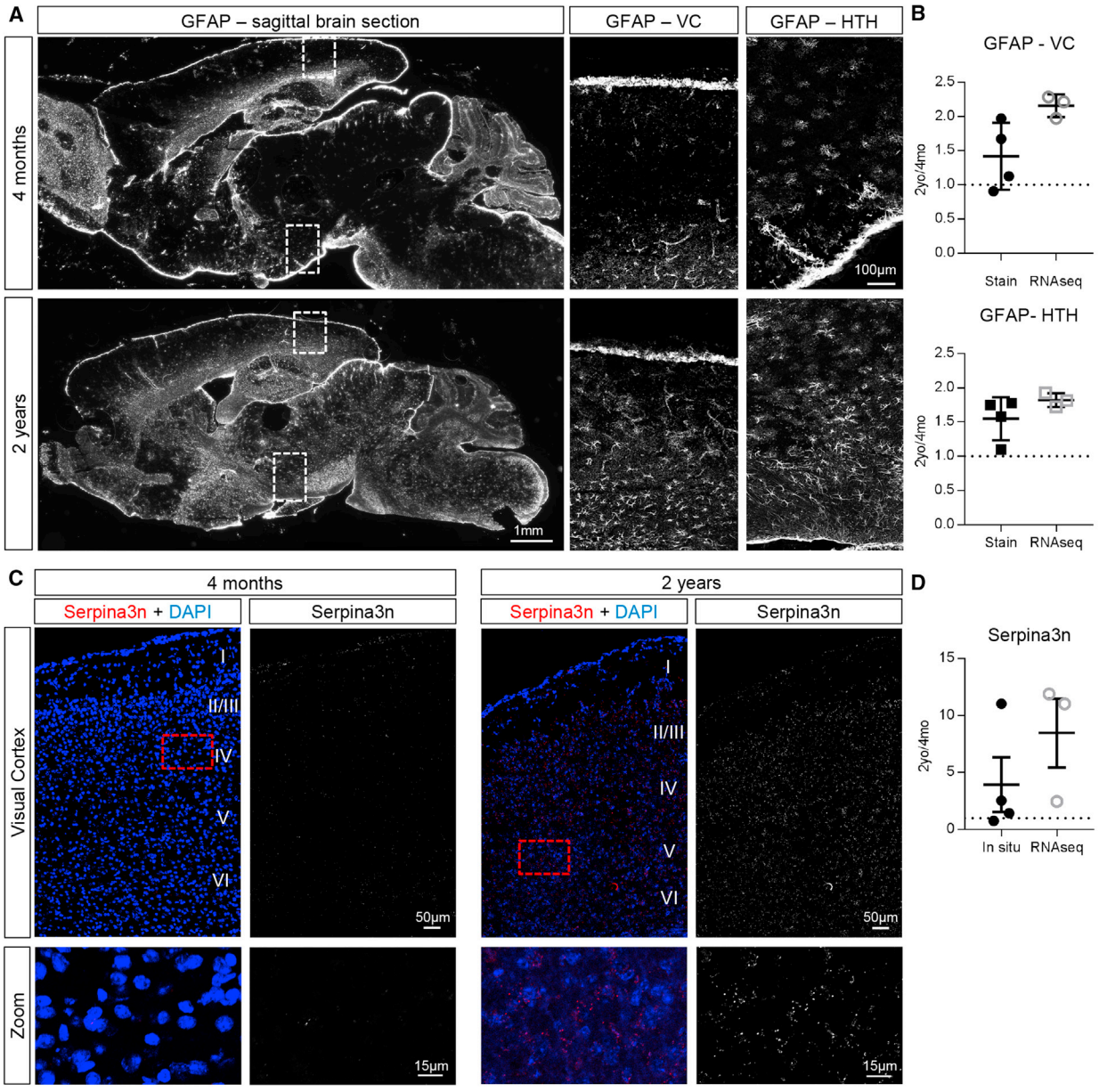


*(legend on next page)*

in HTH, MC, and CB astrocytes and the majority of the genes involved in cholesterol synthesis (Martin et al., 2010) decreasing in the HTH. Conversely, expression of genes responsible for cholesterol transport is increased in the CB and HTH (Figure 4E). Astrocytes are a major source of lipid synthesis in the brain and provide neurons with cholesterol, essential for presynaptic vesicle formation (Figure 4A), suggesting that a lack of cholesterol production in aging astrocytes may inhibit the release of neurotransmitter and decrease presynaptic function (Mauch et al., 2001; van Deijk et al., 2017).

Pathways upregulated in aging astrocytes include the complement system, cytokines, and major histocompatibility complex (MHC) (Table S5). MHC class I is upregulated in the CB, HTH, and VC (Figure 4G), and because this pathway presents antigen, its upregulation may be a sign of cellular stress (Cribbs et al., 2012), although, in the developing brain, MHC class I plays a role in promoting synapse elimination (Huh et al., 2000). Multiple components of the classical complement cascade are significantly upregulated in aging astrocytes across brain regions, including *C3* and *C4*, which are upregulated in all astrocytes (Figure 4F). In development, synapse elimination is induced by complement, with *C1q* tagging synapses for elimination (Stevens et al., 2007) and recruiting *C3*, leading to phagocytosis of synapses by microglia (Schafer et al., 2012). These pathway changes show that aging astrocytes provide an environment that allows synapse elimination via upregulation of complement and MHC and decrease synaptic support by downregulation of cholesterol synthesis.

## Aging Astrocyte Gene Changes Overlap with Reactive Astrocyte Gene Changes

The analysis of individual genes and pathways upregulated in aging astrocytes revealed changes associated with reactive astrocytes, including upregulation of *Gfap*, *Serpina3n*, the complement cascade, and cytokines (Sofroniew, 2015; Zamanian et al., 2012). These changes persist on the level of protein, with immunohistochemistry against Gfap showing an ~1.5 fold increase between 4-month- and 2-year-old VC and HTH, a similar upregulation to that detected by RNA-seq (Figures 5A and 5B). We additionally asked whether *Serpina3n* is upregulated in aging astrocytes using *in situ* hybridization and found a 4-fold upregulation of *Serpina3n* in the VC, similar to that detected by RNA-seq (Figures 5C and 5D). Increases in Gfap and *Serpina3n* are distributed throughout the brain, showing a general increase in astrocyte reactivity across the brain with age rather than a localized response to injury or damage.

Reactive astrocytes are characterized by altered expression of hundreds of genes, not just an upregulation of *Gfap*, and show varying gene expression changes depending on the type and severity of the insult (Sofroniew, 2015; Zamanian et al., 2012). We therefore compared changes in aging astrocytes with those induced by different injury paradigms: peripheral lipopolysaccharide (LPS) to induce neuroinflammation (purportedly damaging reactivity) and middle cerebral artery occlusion (MCAO) to induce a stroke (purportedly protective reactivity) (datasets from Zamanian et al., 2012). We first looked at pan-reactive astrocyte genes (upregulated in response to both LPS and MCAO) and found that between 8% and 56% of genes are significantly upregulated in aging astrocytes, with the MC showing the least changes and the CB the most (Figure 5E). We then investigated changes unique to each paradigm and again identified overlap between the genes increased in aging and the modality-specific reactive astrocyte genes, with most changes in the CB and the least in cortical astrocytes (Figures 5F and 5G). Our data show that aging astrocytes have gene expression changes that partially overlap with reactive astrocyte changes, reflecting a mild to moderate reactive state.

## Adult Cortical Astrocytes Show Region-Dependent Gene Expression

In addition to identifying alterations in gene expression in aging astrocytes, our dataset allows us to determine how astrocytes differ between regions of the adult brain. We concentrated on differences within cortical regions (Figure 6) and between the cortex (CTX) and other brain regions (Figure 7). We added a 4-month somatosensory cortex (SC) condition to enable comparison of 3 distinct cortical areas (Figure 6A); SC samples exhibit 6-fold astrocyte enrichment over input and depletion of other cell types (Figure 6B; Table S1). Clustering analysis using the top expressed genes demonstrated that each cortical region clusters separately from other cortical regions, indicating region-specific astrocyte gene expression (Figure 6C). We determined the number of genes that significantly change between astrocytes in different cortical regions (Table S6), and, to identify astrocyte-specific genes, we filtered for genes that are significantly altered (adjusted $p < 0.05$), expressed at an appreciable level (FPKM > 1), and astrocyte-specific (pull-down/input > 3) (Experimental Procedures; Table S7). MC and VC astrocytes

**Figure 5. Aging Astrocytes Upregulate Expression of Genes that Overlap with Reactive Astrocytes**

(A) Immunohistochemistry for Gfap in 4-month (top) and 2-year (bottom) mouse brain demonstrates increased Gfap protein in multiple regions (VC and HTH) of the aging brain; overview images are mosaic of tile images acquired at 10x (left) and zoomed-in images are cropped from mosaic of tiles acquired at 20x (right).

(B) Quantification of Gfap immunostaining in the VC (top) and HTH (bottom) compared with RNA-seq.

(C) *In situ* hybridization for *Serpina3n* in 4-month (left) and 2-year (right) VC demonstrates increased *Seprina3n* in the aging VC. Images are mosaic of tiles acquired at 20x.

(D) Quantification of *Serpina3n* mRNA in the VC, comparing *in situ* hybridization with RNA-seq.

(B and D) Data are presented as scatterplots of individual points with mean ± SEM. Immunostaining and *in situ*, n = 4 4-month-old and 4 2-year-old mice; RNA-seq, n = 3 4-month-old and 3 2-year-old mice.

(E–G) Comparison of fold change in expression of reactive astrocyte genes between adult and aging astrocytes shows that overlap varies by brain region.

(E) Pan-reactive astrocyte genes.

(F) LPS-specific reactive astrocyte genes.

(G) MCAO-specific reactive astrocyte genes.

Heatmaps are presented as 2-year/4-month (log2) fold change for each brain region. *, significantly altered between 2-year and 4-month astrocytes.

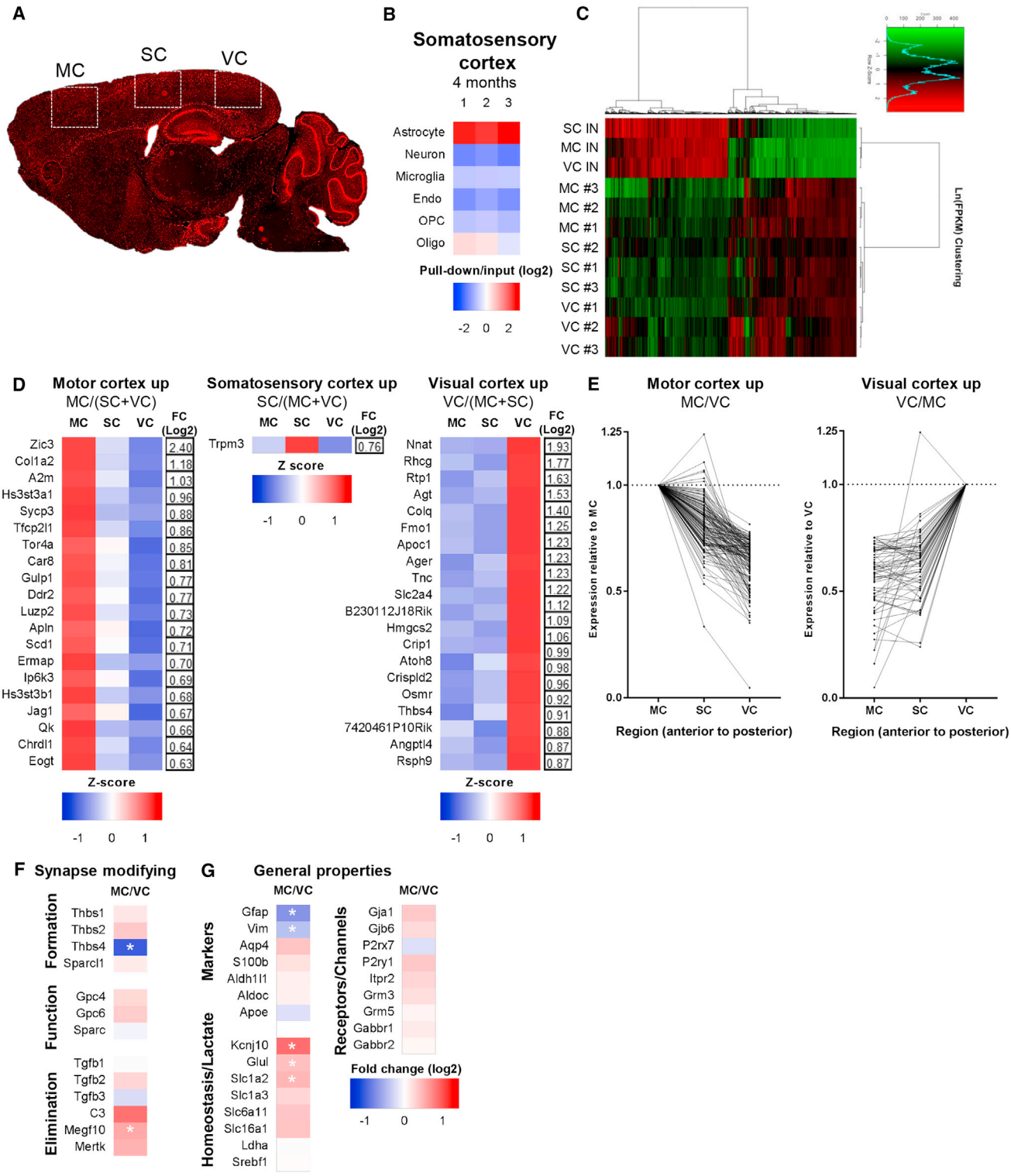


**Figure 6. Adult Cortical Astrocytes Show Region-Dependent Gene Expression**

(A) Schematic of cortical regions examined at 4 months. MC and VC, same as before; somatosensory cortex (SC), new.

(B) Analysis of RNA-seq data for cell-specific mRNA demonstrates enrichment for SC astrocytes over other cell types in the pull-down (astrocyte mRNA) compared with input (total mRNA) (see Table S1 for the gene list).

*(legend continued on next page)*

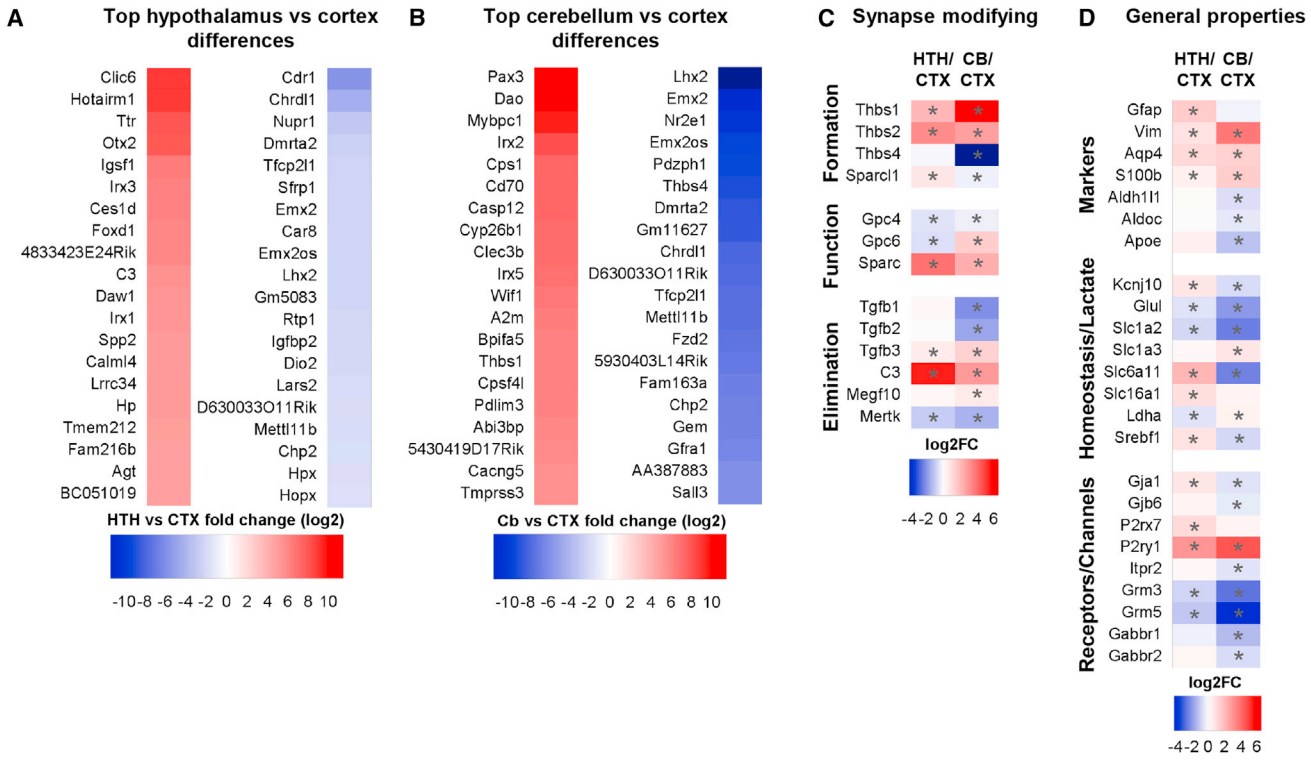


**Figure 7. Regional Differences between Adult Astrocytes**

(A and B) Heatmaps of the top 20 regional astrocyte-enriched genes between adult regions, presented as log2 fold change of HTH (A) or CB (B) FPKM/combined CTX FPKM (see Table S7 for the full list).

(C and D) Comparison of expression of genes that are important for astrocyte regulation of synapses (C) and for astrocyte functions (D), between the HTH and CTX, and CB and CTX, presented as log2 fold change of HTH or CB/CTX. *, significantly altered between regions.

See also Tables S6, S7, and S8.

have the most differences in gene expression compared to all other cortical astrocytes, with 102 and 112 genes upregulated, respectively (Figure 6D; Table S7). SC astrocytes have the least region-specific genes, with an intermediate gene expression profile reflective of their anatomical position between the VC and the MC (Figure 6C). We further generated a list of genes with differential expression comparing the VC to the MC (Table S7) and found that SC astrocyte gene expression is between that of the MC and VC for 93% of the 227 significantly changed astrocyte-enriched genes between the MC and VC (Figure 6E), demonstrating an anterior-to-posterior gene expression gradient in cortical astrocytes for these genes.

We then asked whether cortical astrocytes from distinct regions have differential expression of synapse-modifying genes (Figures 4A and 4C). Because of the expression gradient, we compared expression between MC and VC astrocytes (Table S7; Figures 6F and 6G). VC astrocytes show significantly increased expression of the cytoskeletal protein *Gfap*, the synapse inducer *Thbs4*, and a synapse-eliminating complement cascade component, *C4b*. MC astrocytes express significantly higher levels of the glutamate uptake transporter *Slc1a2* (*Glt1*), the potassium channel *Kcnj10* (*Kir4.1*), and the monoamine oxidase *Maoa*, all of which could affect ongoing synaptic transmission. Additionally, MC astrocytes have increased *Gpc5*, which may affect synaptic function, as well as phagocytic receptor *Megf10*, involved in synapse elimination. Therefore, even within the cortex, astrocytes show differential expression of synapse-regulating genes.

(C) Clustering analysis of the top 3,487 expressed genes shows that astrocyte-ribotag pull-down samples cluster by cortical region. n = 3 4-month-old mice per region.

(D) Heatmaps and fold change of the top 20 genes significantly upregulated in astrocytes in individual cortical regions compared with all other cortical regions (MC, SC, and VC), presented as row *Z* score.

(E) Genes significantly differentially expressed between the MC versus VC show a gradient of gene expression, normalized to the MC (left) or VC (right). One gene (*Cdr1*) exceeds the axis range and is excluded for clarity (see Table S7 for the full list).

(F and G) Heatmap of synapse-modifying (F) and general astrocyte property (G) gene expression changes between the MC and VC, expressed as log2 (fold change). *, significantly altered between regions.

See also Tables S1, S6, S7, and S8.

### Identification of Regionally Enriched Genes in Adult Astrocytes

We next focused on astrocyte-enriched gene expression differences between astrocytes from distinct brain regions. Comparing the CTX and HTH, there are 748 astrocyte-enriched genes significantly upregulated in the HTH and 158 significantly upregulated in the CTX (Table S7; Figure 7A). HTH astrocytes express higher levels of synapse-modifying genes (Figures 4A and 7C), with *Sparc* expression 15-fold greater, *Thbs1* and *2* 4-fold increased, and hevin (*Sparcl1*) significantly increased. *Gpc4* and *6*, however, show significantly lower expression in HTH astrocytes than in CTX astrocytes. HTH astrocytes have increased mRNA for complement factors involved in synapse elimination, *C3* (44-fold) and *C4b* (4.8-fold), and a significant decrease in the phagocytic receptor *Mertk*. In the HTH, the astrocyte water channel *Aqp4* is doubled, the astrocyte marker *Gfap* is increased 3-fold, and the purinoreceptors *P2rx7* and *P2ry4* are significantly increased (Figures 4C and 7D). The primary astrocyte GABA/glycine transporters Gat3 (*Slc6a11*), *Slc6a9*, and Gat1 (*Slc6a1*) are enriched in the HTH, whereas the glutamate transporter Glt1 (*Slc1a2*) is enriched in the CTX (Figure 7D). Pathway analysis of differentially expressed genes (Table S8) identified "metabolism of lipids and lipoproteins" as enriched in the HTH, whereas CTX astrocytes are enriched for "cholesterol biosynthesis" and "steroid metabolism," suggesting differential lipid processing and synaptic support between the two brain regions.

We carried out the same comparison between CTX and CB astrocytes, identifying 326 astrocyte-enriched genes increased in the CB, with 656 genes upregulated in the CTX (Table S7; Figure 7B). Synapse-modifying genes also differ between the regions (Figure 7C), with *Thbs4* expressed over 500-fold more in the CTX and *Thbs1* and *2*, *Gpc6*, and *Sparc* higher in the CB. CTX astrocytes express more Wnt genes (e.g., *Lrp4* and the frizzled family members *Sfrp1*, *Sfrp5*, *Fzd2*, and *Fzd10*), which have been implicated in remodeling adult synapses and may confer neuroprotective benefits in aging (Oliva et al., 2013). The neurotransmitter transporters Glt1 (*Slc1a2*) and Gat3 (*Slc6a11*) as well as metabotropic glutamate receptors (*Grm3* and *5*) and GABA receptors (*Gabbar1* and *2*) are enriched in CTX astrocytes, whereas the glutamate transporter GLAST (*Slc1a3*) and the ionotropic glutamate receptors GluA1 and 4 (*Gria1,4*) are higher in CB astrocytes (Figure 7D). We finally asked whether these regional differences between adult astrocytes are maintained in the aging brain and confirmed that the majority are (Tables S6 and S7), showing that regional astrocyte identity is largely maintained in aging.

## DISCUSSION

We performed RNA-seq on astrocytes from multiple regions of the adult and aging mouse brain to investigate whether alterations in astrocyte properties lead to the loss of neuronal synapses in aging. We found little change in the expression of synapse supportive factors, except for a decrease in cholesterol synthesis, showing that loss of astrocyte support does not lead to senescence of synapses. Instead, we found that astrocytes upregulate the expression of inflammatory factors that can damage synapses and cause their elimination, demonstrating that astrocytes become actively damaging to synapses in the aging brain. There was variability in the number of genes that changed with age in astrocytes from different brain regions, with cortical astrocytes showing the least changes and cerebellar astrocytes the most. This demonstrates the regional dependency of astrocyte aging, with more alterations in areas that experience cell death (Woodruff-Pak et al., 2010; Zhang et al., 2017). Altogether, we provide a comprehensive and validated analysis of gene expression changes in astrocytes between the healthy adult and aging brain, which we have made available as a resource online. We have focused on changes to astrocytes that may affect synaptic function, the hypothesis we set out to test.

Our adult astrocyte gene expression datasets are in broad agreement with other microarray and RNA-seq profiles of astrocytes from the developing and adult brain (Cahoy et al., 2008; Chai et al., 2017; Doyle et al., 2008; Morel et al., 2017; Zhang et al., 2014). We now add to these resources by extending the analysis to examine aging astrocyte gene expression from multiple brain regions using astrocyte-ribotag and RNA-seq. Ribotag restricts analysis to ribosome-associated mRNAs, which are more likely to be actively being made into proteins, providing a representation of the translational state of the cells, a similar approach to that used by others (Chai et al., 2017; Doyle et al., 2008; Morel et al., 2017). Studies using FACS (Cahoy et al., 2008) or immunopanning (Zhang et al., 2016) to isolate astrocyte mRNA offer the ability to look at the whole transcriptome, including non-coding RNAs, but do not highlight mRNAs that are being functionally utilized and are restricted to RNAs present in the cell body because of the isolation method. A difference between ribotag and bacterial artificial chromosome (BAC) trap as a way of tagging ribosomes is that ribotag only requires transient cre recombinase expression to irreversibly express an HA tag on the endogenous ribosomal Rpl22 subunit (Sanz et al., 2009; Doyle et al., 2008), so after recombination, the production of tagged ribosomes is determined by the normal program of that cell, regardless of cre expression. We have validated that the majority of astrocytes in all brain regions examined (~98%, Figure 1) express tagged ribosomes in the adult brain, and, because adult astrogenesis and astrocyte loss are rare, the population of astrocyte-ribotag cells should remain constant between the adult and aged time points and encompass the majority of cells. This is particularly important to note because we used *Gfap*-cre to induce recombination, and *Gfap* increases in aging astrocytes. In the astrocyte-ribotag model, ~95% of tagged ribosomes are expressed by astrocytes, with the rest in non-astrocyte cells, including a subset of neurons and oligodendrocytes (Figures 1 and 2; Table S1). To focus on gene changes occurring in astrocytes, we restricted our analysis to genes that showed an enrichment in the astrocyte pull-down sample compared with the whole-brain input, which should prevent gene expression changes caused by ribosome tagging in a small subset of other cells from being detected. Finally, as with all large datasets, we encourage users to independently validate genes of interest.

The majority of genes implicated in synaptogenesis in the developing brain are unchanged between adult and aging astrocytes. It is surprising that so many of these genes, including those for hevin, thrombospondin, and glypican family members, remain expressed throughout life, long after developmental

synapse formation has ceased. This points to additional roles for these factors in the adult brain, perhaps in relation to learning and memory. The decreased thrombospondin expression in the HTH with aging may contribute to alterations in synapse number and dendritic spine morphology observed with age, as thrombospondins regulate these features (Christopherson et al., 2005). A similar stability of gene expression between the adult and aging brain was found for synaptic transmission regulators, including potassium channels and neurotransmitter uptake transporters. This lack of age-dependent changes points against dysregulated astrocyte homeostasis being involved in altered synaptic transmission in aging.

We found that substantially more genes increase with age than decrease, a trend that mirrors whole-brain data (Cribbs et al., 2012). Of the consistent decreases, the most robust is in the cholesterol synthesis pathway. The brain synthesizes the majority of the cholesterol it needs *in situ* because circulating cholesterol is unable to readily cross the blood-brain barrier. The aging human and rodent brain have decreased cholesterol levels, but the reasons for this decrease are not known (Martin et al., 2010; Thelen et al., 2006). We identified decreased expression of cholesterol synthesis genes, with a significant decrease in the rate-limiting enzyme Hmgcr in aging astrocytes across brain regions, providing a potential mechanism for decreased cholesterol levels in the aging brain. Astrocyte-derived cholesterol is essential for neuronal dendritic elaboration and presynaptic function during development (Mauch et al., 2001), and, given that dendrites atrophy and presynaptic release decreases in the aging brain, decreased astrocyte cholesterol synthesis with age may contribute to these deficits.

A major change we detected in aging astrocytes was an upregulation of genes that have an important role in eliminating excess synapses during development, including the complement pathway and MHC class I (Huh et al., 2000; Stevens et al., 2007). Recently, these same pathways have been implicated in synapse elimination in neurological disorders; for example, *C4* is upregulated in schizophrenia, and complement is involved in eliminating synapses in Alzheimer's disease (Hong et al., 2016; Sekar et al., 2015, 2016). These pathways are among the top genes we find upregulated in astrocytes in the aging brain across regions, strongly suggesting that aging astrocytes provide an environment that is permissive for synapse elimination. Interestingly, the mechanism of synapse elimination involves complement tagging of synapses for phagocytosis by microglia, showing a potential for cross-talk between different glial cell types in aging, which may be bidirectional (Liddelow et al., 2017; Schafer et al., 2012). Microglia also show alterations in gene expression in the aging brain, and, as with astrocytes, these changes vary by brain region, with cerebellar microglia showing the most changes with age, the same result we found for astrocytes (Grabert et al., 2016). The cerebellum is the only region of the brain where age-dependent neuronal death is observed and the only region with astrocyte accumulation of lipofuscin (Figure S3), so it is interesting that this is where the most gene expression changes in glial cells occur. In the future, it will be important to investigate whether glial gene expression changes are causative, preceding Purkinje neuron death, or occur later, as a response to the change in environment caused by neuronal loss.

We find that astrocytes in the aging brain exhibit gene expression changes consistent with reactive astrocytes, albeit with changes of a lesser magnitude, showing a mild to moderate level of reactivity (Sofroniew, 2015). Previous studies have shown increased *Gfap* levels in the aging brain (Bellaver et al., 2017); however, *Gfap* is just one of hundreds of genes that can be upregulated in reactive astrocytes, so our data allowed us to investigate how reactive aging astrocytes are. This analysis identified differential gene expression changes between normal aging and pathological astrocytes, providing a resource to distinguish between astrocytes in healthy aging and disease (Berchtold et al., 2014; Sekar et al., 2015). Interestingly the top 2 genes upregulated by aging in all regions were the reactive astrocyte genes *Serpina3m* and *n*, variations in which have been associated with cognitive function in human aging and Alzheimer's disease vulnerability (Cluett et al., 2010). The cause of the moderate reactivity of astrocytes in the aging brain is unclear because the gene expression changes overlap with those induced by both peripheral inflammation, which induces inflammatory reactive astrocytes, and stroke, which induces purportedly protective reactive astrocytes. Given that many of the upregulated genes reflect inflammatory changes, however, it is interesting that treatment with low doses of the anti-inflammatory drug ibuprofen is protective against aging-induced cognitive deficits in rodents, raising the possibility that a contributing factor in this protection is a reduction in astrocyte reactivity (Rogers et al., 2017).

In the adult brain, we identified significant differences in gene expression between astrocytes in different cortical regions, showing that, even within the cortex, astrocytes may be specialized to regulate the functions of each cortical area. Interestingly, the majority of differentially expressed genes show a gradient of expression across the cortex. These include synapse regulators such as *Thbs4*, which induces synapse formation, and *C4b* and *Megf10*, which eliminate synapses, extracellular matrix factors, and enzymes that process neurotransmitters. When we compared astrocytes from distinct brain regions, many more differences in gene expression were found. Hypothalamic astrocytes express higher levels of genes that regulate synapses compared with cortical astrocytes, indicative of a continued role for astrocytes in adult synaptogenesis in the HTH (Theodosis et al., 2008). Interestingly, hypothalamic astrocytes are enriched in genes involved in lipid metabolism, whereas cortical astrocytes are enriched in genes for lipid synthesis, suggesting different lipid processing between the two areas. Further, adult cerebellar astrocytes are enriched for inflammatory caspases, which may contribute to the greater aging response observed in these cells.

Overall, we find that astrocytes in the aging brain alter their gene expression to produce an environment that will allow synapse elimination and decrease presynaptic function. It has been proposed that aging changes predispose the brain to diseases of aging such as Alzheimer's disease and Parkinson's disease by providing conditions that allow them to develop and progress. Our data support this hypothesis and show that changes in astrocytes could be major contributors. This

suggests that targeting astrocytes is a viable approach to protect synapses in the aging brain and in aging-related diseases.

## EXPERIMENTAL PROCEDURES

All mouse work was approved by the Salk Institute Institutional Animal Care and Use Committee.

### Ribotag Pull-Down

Male mice heterozygous for flox-Rpl22-HA (The Jackson Laboratory, 011029) and hemizygous for *Gfap*-cre (The Jackson Laboratory, 012886) (astrocyte-ribotag) were used to isolated astrocyte mRNA based on a modified ribotag protocol (Sanz et al., 2009). Astrocyte-ribotag mice were aged for either 4 months or 2 years, and the VC, MC, SC, HTH, and CB were micro-dissected on ice in chilled physiological buffer using an adult brain reference atlas (www.brain-map.org) and neuroanatomical landmarks to identify regions (n = 3 mice, 4 months; 3 mice, 2 years).

### RNA-Seq Library Generation and Sequencing

RNA quantity and quality were measured with a Tape Station (Agilent) and Qubit fluorimeter (Thermo Fisher Scientific); see the Supplemental Experimental Procedures for RIN integrity number (RIN) scores. 100–400 ng of RNA was used to make libraries; to avoid batch effects, library preparation and sequencing were done at the same time for all samples. mRNA was extracted with oligo-dT beads, capturing poly(A) tails, and cDNA libraries were made with the Illumina TruSeq Stranded mRNA Library Preparation Kit (RS-122-2101) by the Salk Institute Next Generation Sequencing (NGS) Core. Samples were sequenced on an Illumina HiSeq 2500 with single-end 50-bp reads at 25–60 million reads per sample.

### RNA-Seq Mapping, Analysis, and Statistics

Raw sequencing data were demultiplexed and converted into FASTQ files using consensus assessment of sequence and variation (CASAVA) (v1.8.2) and quality-tested with FASTQC v0.11.2. Analysis was done in R v3.1.1 with Bioconductor package v2.13. Alignment to the mm10 genome was performed using the spliced transcripts alignment to a reference (STAR) aligner, version 2.4.0k (Dobin et al., 2013). Mapping was carried out using default parameters (up to 10 mismatches per read and up to 9 multi-mapping locations per read), and a high ratio of uniquely mapped reads (> 75%) was confirmed, with exonic alignment inspected to ensure that reads were mapped predominantly to annotated exons. Raw gene expression was quantified across all genes (RNA-seq) using the top-expressed isoform as a proxy for gene expression, and differential gene expression was carried out using the EdgeR package, version 3.6.8, with default normalization, using replicates to compute within-group dispersion and, when cortical samples were pooled, batch correction to account for the differences between mice (Robinson et al., 2010). The standard EdgeR normalization and differential expression pipeline was used to ensure that mean-variance relationships were appropriately modeled prior to differential expression testing. Significance for differential expression was defined as adjusted $p < 0.05$, calculated with EdgeR using Benjamini-Hochberg's procedure for multiple comparisons adjustment.

### Characterization of Astrocyte-Ribotag

To determine the astrocyte specificity of the astrocyte-ribotag line, we performed 2 analyses: immunostaining against the ribotag epitope (HA) and cell type-specific markers (astrocytes, microglia, oligodendrocytes, neurons, and oligodendrocyte precursor cells) and qRT-PCR for cell type-specific mRNA from the ribotag pull-down compared with the input.

### *In Situ* Hybridization

The RNAscope 2.5 HD Multiplex Fluorescent Manual Assay kit (ACDbio, 320850) was used with modifications to detect mRNA changes between 4-month- and 2-year-old mice. 4 mice (biological replicates) were analyzed per time point, with 3 brain sections/animal/probe (technical replicates) imaged on a confocal microscope, and the amount of signal was quantified in Imaris (Bitplane). See the Supplemental Experimental Procedures for further details.

## DATA AND SOFTWARE AVAILABILITY

The accession number for the sequencing data reported in this paper is GEO: GSE99791. Analyzed reads (FPKM) are available from the GEO, http://igc1.salk.edu:3838/astrocyte_aging_transcriptome/, and Table S2.

## SUPPLEMENTAL INFORMATION

Supplemental Information includes Supplemental Experimental Procedures, four figures, and eight tables and can be found with this article online at https://doi.org/10.1016/j.celrep.2017.12.039.

## ACKNOWLEDGMENTS

We thank Alex Kopelevich and Cari Dowling for technical support, Luisa Amaral for website design and construction, Mat LeBlanc and Ye Zheng for advice, the NIA for aged WT mice, and members of the Allen lab and MNL for discussions. This project was funded by an Ellison Medical Foundation New Scholar in Aging Award (to N.J.A.). M.M.B. received support from the Chapman Foundation. Work in the lab of N.J.A. is supported by NIH-NINDS R01 NS089791 the Hearst Foundation, the Pew Foundation, the Dana Foundation, and the Whitehall Foundation. Work in the Razavi Newman Integrative Genomics and Bioinformatics Core Facility of the Salk Institute is funded by NIH-NCI CCSG P30 014195 and the Helmsley Trust. This work was supported by the NGS Core Facility of the Salk Institute with funding from NIH-NCI CCSG P30 014195, the Chapman Foundation, and the Helmsley Charitable Trust.

## AUTHOR CONTRIBUTIONS

M.M.B. and N.J.A. designed the experiments and wrote the manuscript with input from other authors. N.J.A. conceived the project. M.M.B. performed all experiments except as noted. N.J.A., M.M.B., G.A.E., and M.N.S. analyzed data.

## DECLARATION OF INTERESTS

The authors declare no competing interests.

Received: November 7, 2017
Revised: December 6, 2017
Accepted: December 11, 2017
Published: January 2, 2018

## REFERENCES

Allen, N.J. (2014). Astrocyte regulation of synaptic behavior. Annu. Rev. Cell Dev. Biol. *30*, 439–463.

Allen, N.J., Bennett, M.L., Foo, L.C., Wang, G.X., Chakraborty, C., Smith, S.J., and Barres, B.A. (2012). Astrocyte glypicans 4 and 6 promote formation of excitatory synapses via GluA1 AMPA receptors. Nature *486*, 410–414.

Bellaver, B., Souza, D.G., Souza, D.O., and Quincozes-Santos, A. (2017). Hippocampal Astrocyte Cultures from Adult and Aged Rats Reproduce Changes in Glial Functionality Observed in the Aging Brain. Mol. Neurobiol. *54*, 2969–2985.

Berchtold, N.C., Sabbagh, M.N., Beach, T.G., Kim, R.C., Cribbs, D.H., and Cotman, C.W. (2014). Brain gene expression patterns differentiate mild cognitive impairment from normal aged and Alzheimer's disease. Neurobiol. Aging *35*, 1961–1972.

Bialas, A.R., and Stevens, B. (2013). TGF-β signaling regulates neuronal C1q expression and developmental synaptic refinement. Nat. Neurosci. *16*, 1773–1782.

Bobkova, N.V., Evgen'ev, M., Garbuz, D.G., Kulikov, A.M., Morozov, A., Samokhin, A., Velmeshev, D., Medvinskaya, N., Nesterova, I., Pollock, A., and Nudler, E. (2015). Exogenous Hsp70 delays senescence and improves cognitive function in aging mice. Proc. Natl. Acad. Sci. USA *112*, 16006–16011.

Cahoy, J.D., Emery, B., Kaushal, A., Foo, L.C., Zamanian, J.L., Christopherson, K.S., Xing, Y., Lubischer, J.L., Krieg, P.A., Krupenko, S.A., et al. (2008). A transcriptome database for astrocytes, neurons, and oligodendrocytes: a new resource for understanding brain development and function. J. Neurosci. *28*, 264–278.

Chai, H., Diaz-Castro, B., Shigetomi, E., Monte, E., Octeau, J.C., Yu, X., Cohn, W., Rajendran, P.S., Vondriska, T.M., Whitelegge, J.P., et al. (2017). Neural Circuit-Specialized Astrocytes: Transcriptomic, Proteomic, Morphological, and Functional Evidence. Neuron *95*, 531–549.e9.

Christopherson, K.S., Ullian, E.M., Stokes, C.C., Mullowney, C.E., Hell, J.W., Agah, A., Lawler, J., Mosher, D.F., Bornstein, P., and Barres, B.A. (2005). Thrombospondins are astrocyte-secreted proteins that promote CNS synaptogenesis. Cell *120*, 421–433.

Chung, W.-S., Clarke, L.E., Wang, G.X., Stafford, B.K., Sher, A., Chakraborty, C., Joung, J., Foo, L.C., Thompson, A., Chen, C., et al. (2013). Astrocytes mediate synapse elimination through MEGF10 and MERTK pathways. Nature *504*, 394–400.

Cluett, C., Brayne, C., Clarke, R., Evans, G., Matthews, F., Rubinsztein, D.C., Huppert, F., Llewellyn, D.J., Rice, N., Henley, W., et al. (2010). Polymorphisms in LMNA and near a SERPINA gene cluster are associated with cognitive function in older people. Neurobiol. Aging *31*, 1563–1568.

Cribbs, D.H., Berchtold, N.C., Perreau, V., Coleman, P.D., Rogers, J., Tenner, A.J., and Cotman, C.W. (2012). Extensive innate immune gene activation accompanies brain aging, increasing vulnerability to cognitive decline and neurodegeneration: a microarray study. J. Neuroinflammation *9*, 179.

Dobin, A., Davis, C.A., Schlesinger, F., Drenkow, J., Zaleski, C., Jha, S., Batut, P., Chaisson, M., and Gingeras, T.R. (2013). STAR: ultrafast universal RNA-seq aligner. Bioinformatics *29*, 15–21.

Doyle, J.P., Dougherty, J.D., Heiman, M., Schmidt, E.F., Stevens, T.R., Ma, G., Bupp, S., Shrestha, P., Shah, R.D., Doughty, M.L., et al. (2008). Application of a translational profiling approach for the comparative analysis of CNS cell types. Cell *135*, 749–762.

Garcia, A.D.R., Doan, N.B., Imura, T., Bush, T.G., and Sofroniew, M.V. (2004). GFAP-expressing progenitors are the principal source of constitutive neurogenesis in adult mouse forebrain. Nat. Neurosci. *7*, 1233–1241.

Goodman, T., and Hajihosseini, M.K. (2015). Hypothalamic tanycytes-masters and servants of metabolic, neuroendocrine, and neurogenic functions. Front. Neurosci. *9*, 387.

Grabert, K., Michoel, T., Karavolos, M.H., Clohisey, S., Baillie, J.K., Stevens, M.P., Freeman, T.C., Summers, K.M., and McColl, B.W. (2016). Microglial brain region-dependent diversity and selective regional sensitivities to aging. Nat. Neurosci. *19*, 504–516.

Gray, D.A., and Woulfe, J. (2005). Lipofuscin and aging: a matter of toxic waste. Sci. SAGE KE *2005*, re1.

Hong, S., Beja-Glasser, V.F., Nfonoyim, B.M., Frouin, A., Li, S., Ramakrishnan, S., Merry, K.M., Shi, Q., Rosenthal, A., Barres, B.A., et al. (2016). Complement and microglia mediate early synapse loss in Alzheimer mouse models. Science *352*, 712–716.

Huh, G.S., Boulanger, L.M., Du, H., Riquelme, P.A., Brotz, T.M., and Shatz, C.J. (2000). Functional requirement for class I MHC in CNS development and plasticity. Science *290*, 2155–2159.

Jiang, T., and Cadenas, E. (2014). Astrocytic metabolic and inflammatory changes as a function of age. Aging Cell *13*, 1059–1067.

Khakh, B.S., and Sofroniew, M.V. (2015). Diversity of astrocyte functions and phenotypes in neural circuits. Nat. Neurosci. *18*, 942–952.

Kucukdereli, H., Allen, N.J., Lee, A.T., Feng, A., Ozlu, M.I., Conatser, L.M., Chakraborty, C., Workman, G., Weaver, M., Sage, E.H., et al. (2011). Control of excitatory CNS synaptogenesis by astrocyte-secreted proteins Hevin and SPARC. Proc. Natl. Acad. Sci. USA *108*, E440–E449.

Liddelow, S.A., Guttenplan, K.A., Clarke, L.E., Bennett, F.C., Bohlen, C.J., Schirmer, L., Bennett, M.L., Münch, A.E., Chung, W.-S., Peterson, T.C., et al. (2017). Neurotoxic reactive astrocytes are induced by activated microglia. Nature *541*, 481–487.

Martin, M., Dotti, C.G., and Ledesma, M.D. (2010). Brain cholesterol in normal and pathological aging. Biochim. Biophys. Acta *1801*, 934–944.

Mauch, D.H., Nägler, K., Schumacher, S., Göritz, C., Müller, E.C., Otto, A., and Pfrieger, F.W. (2001). CNS synaptogenesis promoted by glia-derived cholesterol. Science *294*, 1354–1357.

Morel, L., Chiang, M.S.R., Higashimori, H., Shoneye, T., Iyer, L.K., Yelick, J., Tai, A., and Yang, Y. (2017). Molecular and Functional Properties of Regional Astrocytes in the Adult Brain. J. Neurosci. *37*, 8706–8717.

Oliva, C.A., Vargas, J.Y., and Inestrosa, N.C. (2013). Wnts in adult brain: from synaptic plasticity to cognitive deficiencies. Front. Cell. Neurosci. *7*, 224.

Orre, M., Kamphuis, W., Osborn, L.M., Melief, J., Kooijman, L., Huitinga, I., Klooster, J., Bossers, K., and Hol, E.M. (2014). Acute isolation and transcriptome characterization of cortical astrocytes and microglia from young and aged mice. Neurobiol. Aging *35*, 1–14.

Pannese, E. (2011). Morphological changes in nerve cells during normal aging. Brain Struct. Funct. *216*, 85–89.

Peek, S.L., Mah, K.M., and Weiner, J.A. (2017). Regulation of neural circuit formation by protocadherins. Cell. Mol. Life Sci. *74*, 4133–4157.

Pelvig, D.P., Pakkenberg, H., Stark, A.K., and Pakkenberg, B. (2008). Neocortical glial cell numbers in human brains. Neurobiol. Aging *29*, 1754–1762.

Robinson, M.D., McCarthy, D.J., and Smyth, G.K. (2010). edgeR: a Bioconductor package for differential expression analysis of digital gene expression data. Bioinformatics *26*, 139–140.

Rogers, J.T., Liu, C.-C., Zhao, N., Wang, J., Putzke, T., Yang, L., Shinohara, M., Fryer, J.D., Kanekiyo, T., and Bu, G. (2017). Subacute ibuprofen treatment rescues the synaptic and cognitive deficits in advanced-aged mice. Neurobiol. Aging *53*, 112–121.

Sakers, K., Lake, A.M., Khazanchi, R., Ouwenga, R., Vasek, M.J., Dani, A., and Dougherty, J.D. (2017). Astrocytes locally translate transcripts in their peripheral processes. Proc. Natl. Acad. Sci. USA *114*, E3830–E3838.

Samson, R.D., and Barnes, C.A. (2013). Impact of aging brain circuits on cognition. Eur. J. Neurosci. *37*, 1903–1915.

Sanz, E., Yang, L., Su, T., Morris, D.R., McKnight, G.S., and Amieux, P.S. (2009). Cell-type-specific isolation of ribosome-associated mRNA from complex tissues. Proc. Natl. Acad. Sci. USA *106*, 13939–13944.

Schafer, D.P., Lehrman, E.K., Kautzman, A.G., Koyama, R., Mardinly, A.R., Yamasaki, R., Ransohoff, R.M., Greenberg, M.E., Barres, B.A., and Stevens, B. (2012). Microglia sculpt postnatal neural circuits in an activity and complement-dependent manner. Neuron *74*, 691–705.

Sekar, S., McDonald, J., Cuyugan, L., Aldrich, J., Kurdoglu, A., Adkins, J., Serrano, G., Beach, T.G., Craig, D.W., Valla, J., et al. (2015). Alzheimer's disease is associated with altered expression of genes involved in immune response and mitochondrial processes in astrocytes. Neurobiol. Aging *36*, 583–591.

Sekar, A., Bialas, A.R., de Rivera, H., Davis, A., Hammond, T.R., Kamitaki, N., Tooley, K., Presumey, J., Baum, M., Van Doren, V., et al.; Schizophrenia Working Group of the Psychiatric Genomics Consortium (2016). Schizophrenia risk from complex variation of complement component 4. Nature *530*, 177–183.

Sofroniew, M.V. (2015). Astrogliosis. Cold Spring Harb. Perspect. Biol. *7*, a020420.

Soreq, L., Rose, J., Soreq, E., Hardy, J., Trabzuni, D., Cookson, M.R., Smith, C., Ryten, M., Patani, R., and Ule, J.UK Brain Expression Consortium; North American Brain Expression Consortium (2017). Major Shifts in Glial Regional Identity Are a Transcriptional Hallmark of Human Brain Aging. Cell Rep. *18*, 557–570.

Stevens, B., Allen, N.J., Vazquez, L.E., Howell, G.R., Christopherson, K.S., Nouri, N., Micheva, K.D., Mehalow, A.K., Huberman, A.D., Stafford, B., et al. (2007). The classical complement cascade mediates CNS synapse elimination. Cell *131*, 1164–1178.

Thelen, K.M., Falkai, P., Bayer, T.A., and Lütjohann, D. (2006). Cholesterol synthesis rate in human hippocampus declines with aging. Neurosci. Lett. *403*, 15–19.

Theodosis, D.T., Poulain, D.A., and Oliet, S.H.R. (2008). Activity-dependent structural and functional plasticity of astrocyte-neuron interactions. Physiol. Rev. *88*, 983–1008.

van Deijk, A.F., Camargo, N., Timmerman, J., Heistek, T., Brouwers, J.F., Mogavero, F., Mansvelder, H.D., Smit, A.B., and Verheijen, M.H.G. (2017). Astrocyte lipid metabolism is critical for synapse development and function in vivo. Glia *65*, 670–682.

Wang, M., Gamo, N.J., Yang, Y., Jin, L.E., Wang, X.-J., Laubach, M., Mazer, J.A., Lee, D., and Arnsten, A.F.T. (2011). Neuronal basis of age-related working memory decline. Nature *476*, 210–213.

Woodruff-Pak, D.S., Foy, M.R., Akopian, G.G., Lee, K.H., Zach, J., Nguyen, K.P.T., Comalli, D.M., Kennard, J.A., Agelan, A., and Thompson, R.F. (2010). Differential effects and rates of normal aging in cerebellum and hippocampus. Proc. Natl. Acad. Sci. USA *107*, 1624–1629.

Zamanian, J.L., Xu, L., Foo, L.C., Nouri, N., Zhou, L., Giffard, R.G., and Barres, B.A. (2012). Genomic analysis of reactive astrogliosis. J. Neurosci. *32*, 6391–6410.

Zhang, Y., Chen, K., Sloan, S.A., Bennett, M.L., Scholze, A.R., O'Keeffe, S., Phatnani, H.P., Guarnieri, P., Caneda, C., Ruderisch, N., et al. (2014). An RNA-sequencing transcriptome and splicing database of glia, neurons, and vascular cells of the cerebral cortex. J. Neurosci. *34*, 11929–11947.

Zhang, Y., Sloan, S.A., Clarke, L.E., Caneda, C., Plaza, C.A., Blumenthal, P.D., Vogel, H., Steinberg, G.K., Edwards, M.S., Li, G., et al. (2016). Purification and Characterization of Progenitor and Mature Human Astrocytes Reveals Transcriptional and Functional Differences with Mouse. Neuron *89*, 37–53.

Zhang, Y., Kim, M.S., Jia, B., Yan, J., Zuniga-Hertz, J.P., Han, C., and Cai, D. (2017). Hypothalamic stem cells control ageing speed partly through exosomal miRNAs. Nature *548*, 52–57.

**Cell Reports, Volume *22***

## Supplemental Information

# The Aging Astrocyte Transcriptome from Multiple Regions of the Mouse Brain

**Matthew M. Boisvert, Galina A. Erikson, Maxim N. Shokhirev, and Nicola J. Allen**

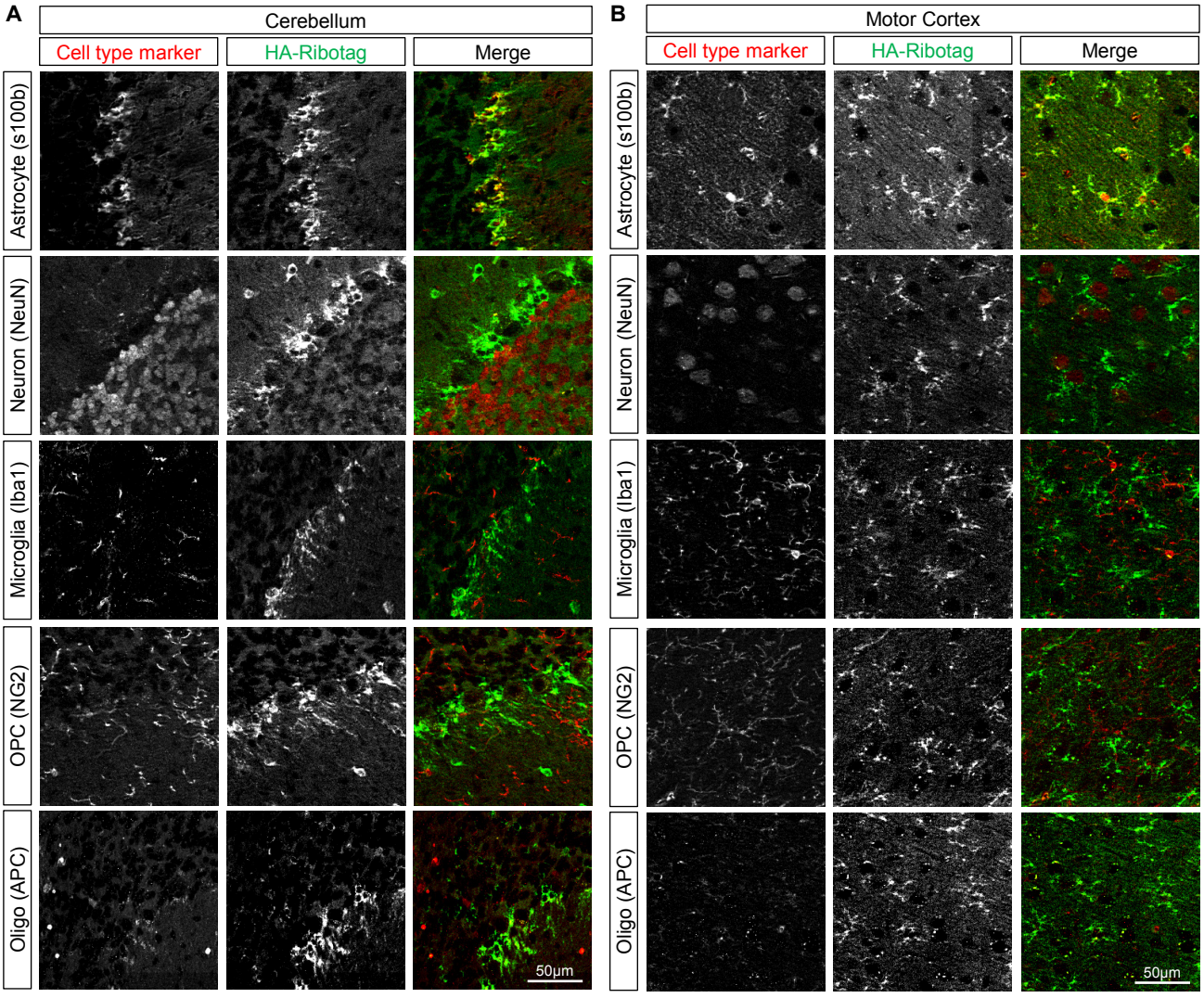


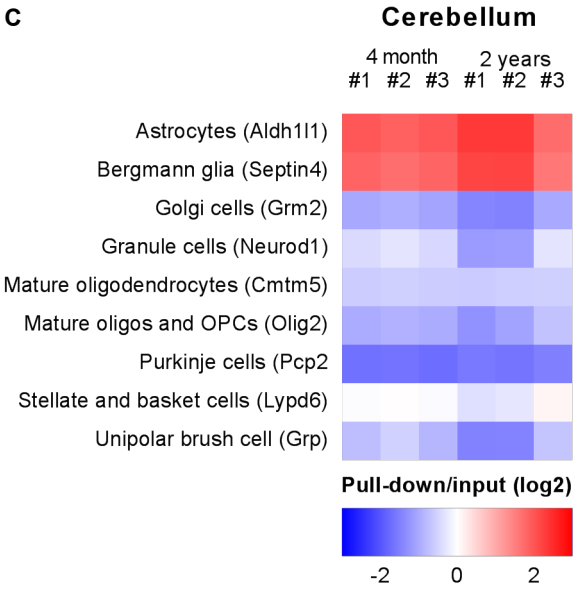


**Figure S1, relates to Figure 1,2. Validation of astrocyte-ribotag model in the cerebellum and motor cortex.** Immunostaining for HA and cell-specific markers, to determine cell-type expression of HA, in the cerebellum (**A**) and motor cortex (**B**). Images shown are cropped from a larger mosaic tiled image **C.** Analysis of cerebellum RNAseq data for cerebellar cell type-specific mRNA, comparing HA-tagged ribosome pulldown mRNA (astrocyte) to the total lysate mRNA (input sample), as in Fig 2, but with cerebellum specific gene lists developed from (Doyle et al., 2008). Cre line from which the pulldown in Doyle data was derived is labeled in parentheses.

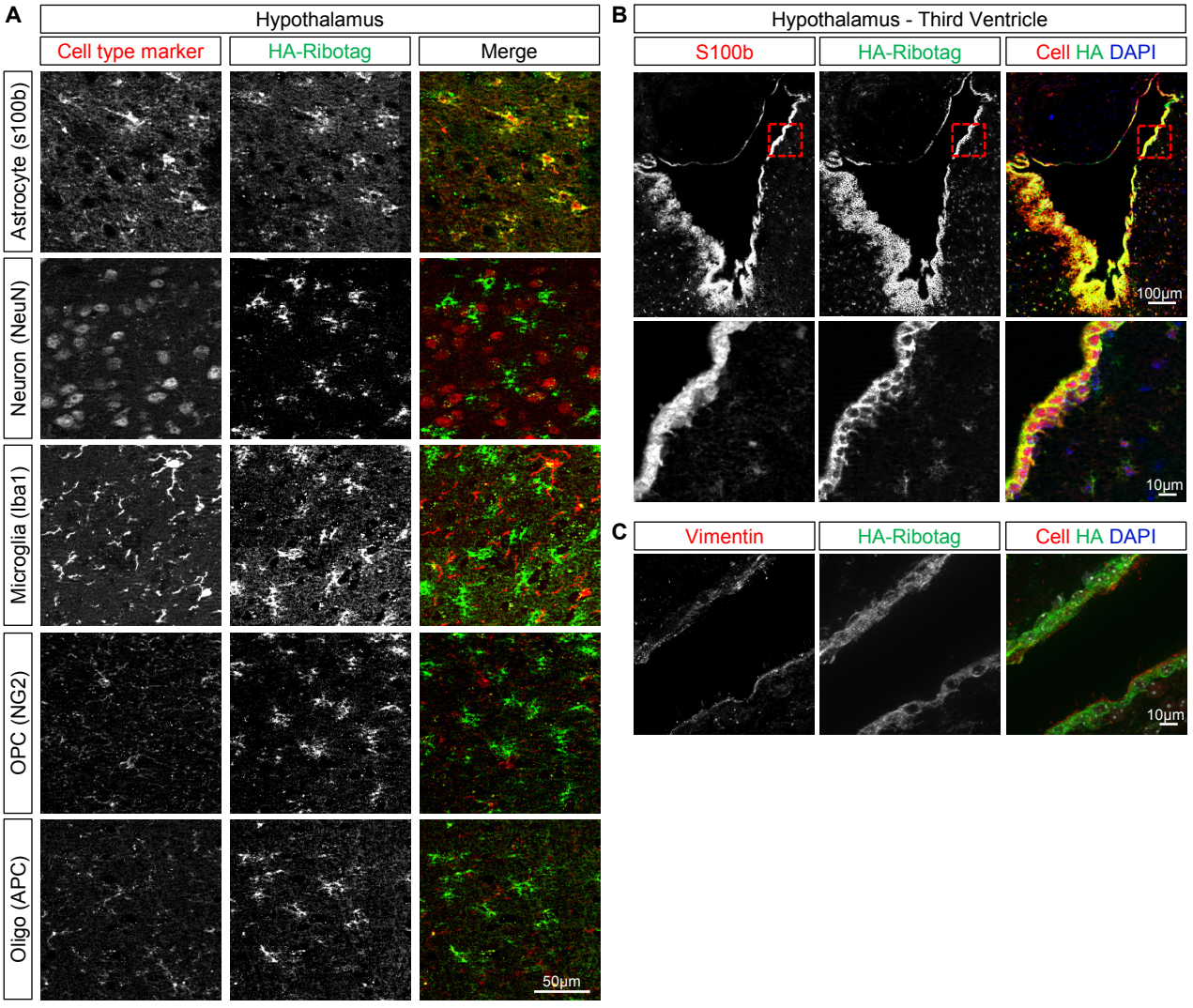


**Figure S2, relates to Figure 1. Validation of astrocyte-ribotag model in the hypothalamus.** Immunostaining for HA and cell-specific markers, to determine cell-type expression of HA in the hypothalamus (**A**). Images shown are cropped from a larger mosaic tiled image **B, C.** Immunostaining for HA and S100b (**B**) or vimentin (**C**) in the third ventricle of the hypothalamus, to detect expression of HA-tagged ribosomes in α-tanycyte/ependymal cells. Box indicates zoom area in **B.**

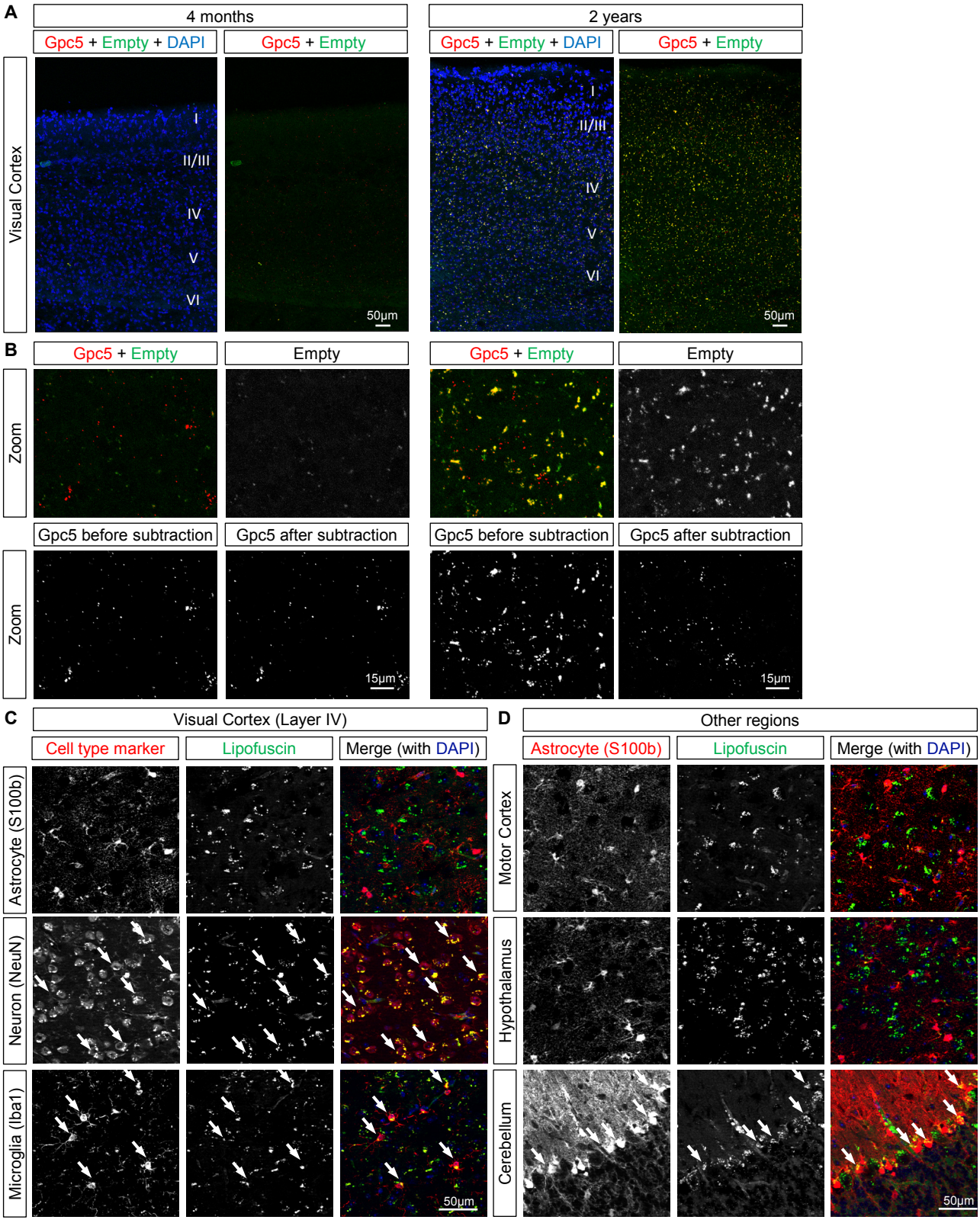


**Figure S3, relates to Figure 3. Subtraction of lipofuscin background from *in situ* samples and lipofuscin cellular localization. A.** Raw images of *in situ* hybridization of *Gpc5* in the visual cortex of 4 month (left) and 2 year old (right) mouse brain (note same example images as Fig S4). Images are mosaic image of tiles acquired at 20x **B.** Images of *Gpc5 in situ* on 4 month (left) and 2 year old (right) cortex with probe and empty (unlabeled channel, with autofluorescence indicative of lipofuscin) channels, alone and merged, with lower right panels showing the *Gpc5* channel after subtracting the "empty" channel. **C,D.** Immunostaining for cell-type markers and lipofuscin (autofluorescence) in 2 year old brain, in layer IV of visual cortex (**C**), and for astrocytes in the motor cortex, hypothalamus, and cerebellum (**D**), with arrows marking example cell-lipofuscin overlap. Images shown are cropped from a larger mosaic tiled image.

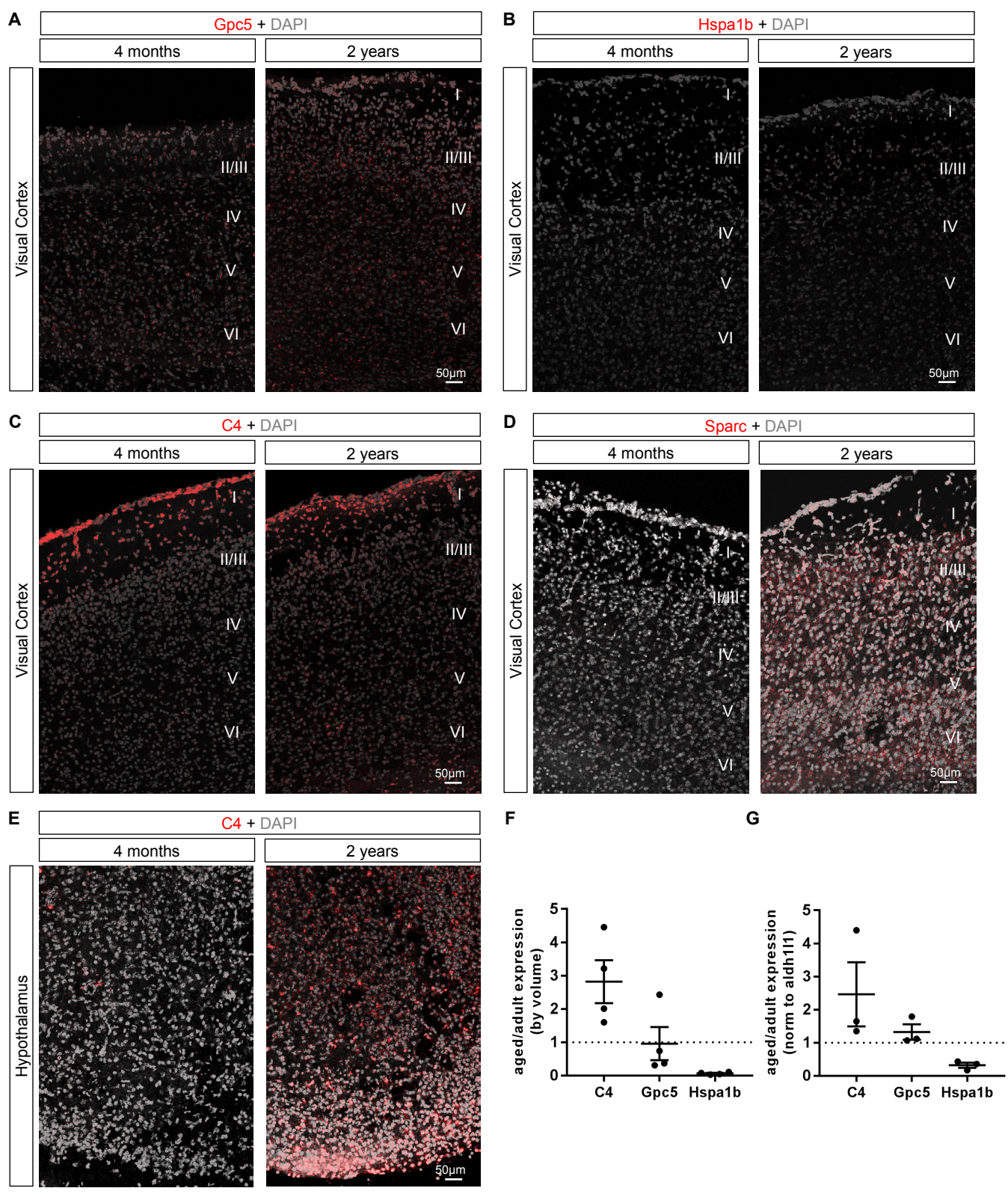


**Figure S4, relates to Figure 3. *In situ* hybridization validation of RNAseq changes.** *In situ* hybridization to detect mRNA for candidate genes in the VC (**A-D**) and HTH (**E**) of 4 month (left) and 2 year old (right) mouse brain, related to Fig 3 example images. Visual cortex RNAscope for *Gpc5* (**A** unchanged in aging; note same example images as Fig S3), *Hspa1b* (**B,** decreased in aging), *C4* and *Sparc* (**C, D**, increased in aging), and hypothalamic *C4* (**E,** increased in aging). Images are mosaic of tiles acquired at 20x **F,G.** Normalization of *in situ* hybridization data from Fig 3 to either total analyzed volume of stain (**F**) or total intensity of *Aldh1l1* colabel (**G**). The direction of gene expression change matches that in Fig 3.

## SUPPLEMENTAL EXPERIMENTAL PROCEDURES

### Mice

All mice were maintained in Salk Institute's animal facility in specific pathogen free group housing with ad libitum access to food and water, on a 12 hour light/12 dark cycle.

***Astrocyte-ribotag mice*** were generated by crossing Gfap-cre hemizygous females (B6.Cg-Tg (GFAP-cre)73.12Mvs/J, Jax #012886) to homozygous flox-Rpl22-HA males (B6N.129-Rpl22tm1.1Psam/J, Jax #011029). Male mice heterozygous for flox-Rpl22-HA and hemizygous for cre (astrocyte-ribotag) were used to purify mRNA for astrocyte-enriched RNAseq experiments, at 4 months of age or 2 years of age.

***C57Bl6/J wild-type (WT) mice*** (Jax #000664) were used to validate changes in astrocyte mRNA expression in aging that were detected using RNAseq. For 2-year-old time points, C57bl6/J male 1.5-year-old mice were imported from the National Institutes of Aging and aged for an additional 6 months in the Salk Institute's mouse colony. 4-month-old mice were either bred in-house or purchased from Jackson Laboratories at 10-12 weeks of age and aged to 4 months in Salk animal facilities.

***Tissue collection.*** Mice were anesthetized with an intraperitoneal injection of 100 mg/kg Ketamine (Victor Medical Company)/20 mg/kg Xylazine (Anased) mix in sterile saline before tissue collection, as outlined below.

### Ribotag

***Brain Dissection*** Mice were anesthetized between 10am-12pm and transcardially perfused with 10ml PBS then 10ml 1% PFA. The animals were inspected by a veterinarian, and no gross abnormalities or pathology detected. Brains were dissected in (2.5mM HEPES-KOH pH 7.4, 35mM glucose, 4mM NaHCO3 in 1x Hank's Balanced Salt Solution with 100µg/ml cycloheximide added fresh (Heiman et al., 2014). Brains were cut from approximately bregma 2.3 to 1.1 (MC), -0.3 to -1.5 (SC), and at -3.4 (VC), with the cortex then carefully detached from the rest of the brain and any visible white matter removed. Lateral cuts were made 2mm from midline on either side for the MC, at 1.5 and 4mm for SC, and at 1mm and 3mm from the midline for the VC section. For the HTH dissection, a region from the bregma -0.3 to -1.5 slice (SC) was cut ~1.2mm from midline and ~1mm from bottom. The cerebellum was dissected off. All brain regions derive from the same biological replicates to minimize spurious interregional variability, as in (Chai et al., 2017; Morel et al., 2017).These regions were flash frozen in liquid nitrogen, and stored at -80°C until isolation of mRNA.

***Ribotag Pulldown*** A modified Ribotag protocol was performed to isolate astrocyte enriched RNA. Briefly, a dounce homogenizer was used to homogenize brain samples in 2ml cycloheximide-supplemented homogenization buffer (1% NP-40, 0.1M KCl, 0.05M Tris, pH 7.4, 0.012M MgCl2 in RNase free water, with 1:1000 1M DTT, 1mg/mL heparin, 0.1mg/mL cycloheximide, 1:100 Protease inhibitors, and 1:200 RNAsin added fresh). Homogenates were centrifuged and the supernatant incubated on a rotator at 4°C for 4 hours with 5ul anti-HA antibody to bind the HA-tagged ribosomes (CST Rb anti-HA #3724, 1:200). Magnetic IgG beads (Thermo Scientific Pierce #88847) were conjugated to the antibody-ribosome complex via overnight incubation on a rotator at 4°C. Samples were washed with a high salt buffer (0.333M KCl, 1% NP40, 1:2000 1M DTT, 0.1mg/mL cycloheximide, 0.05M Tris pH 7.4, 0.012M MgCl2 in RNase-free water), and RNA released from ribosomes with 350uL RLT buffer (from Qiagen RNeasy kit) with 1% BME. RNA was purified using RNeasy Plus Micro kit (Qiagen 74034) according to manufacturer instructions and eluted into 16ul RNase-free water. Eluted RNA was stored at -80°C. For each brain region/age, 50ul of homogenate (pre- anti-HA antibody addition) was set aside after centrifugation, kept at -20°C overnight, and purified via RNeasy Micro kit as an 'input' sample, and used to determine astrocyte enrichment. RIN values: 4mo_VC_1 (7), 4mo_VC_2 (7), 4mo_VC_3 (6.7), 4mo_SC_1 (8), 4mo_SC_2 (8.2), 4mo_SC_3 (8.2), 4mo_MC_1 (6.5), 4mo_MC_2 (7.3), 4mo_MC_3 (7.3), 4mo_HTH_1 (7), 4mo_HTH_2 (6.5), 4mo_HTH_3 (6.5), 4mo_CB_1 (6.3), 4mo_CB_2 (3.7), 4mo_CB_3 (6.4), 2yo_VC_1 (6.5), 2yo_VC_2 (6), 2yo_VC_3 (6.1), 2yo_MC_1 (5.3), 2yo_MC_2 (7.4), 2yo_MC_3 (6.5), 2yo_HTH_1 (6.3), 2yo_HTH_2 (6.1), 2yo_HTH_3 (5.9), 2yo_CB_1 (4.1), 2yo_CB_2 (5.1), 2yo_CB_3 (4.4), 4mo_VC_1_IN (8), 4mo_SC_IN (8.1), 4mo_MC_1_IN (7.9), 4mo_HTH_1_IN (6.5), 4mo_CB_1_IN (8), 2yo_VC_1_IN (6.7), 2yo_MC_1_IN (6.4), 2yo_HTH_2_IN (6.1), 2yo_CB_1_IN (6.2).

### Analysis

***Generation of cell type specific gene lists*** Gene lists were developed from purified cell type RNAseq data from the developing brain (Zhang et al., 2014), selecting genes enriched >10-fold in a given cell type over all other cell types (except for OPCs, which are enriched >10 over all other cell types except newly formed oligodendrocytes), and expressed with FPKM>5 in our input samples. These gene lists were cross-referenced with microarray data from FACS-purified adolescent mouse astrocytes (Cahoy et al., 2008). To ensure astrocyte specificity we excluded any

putative astrocyte marker gene from the Zhang list that showed <2.5-fold enrichment in astrocytes over whole forebrain in the Cahoy list, and excluded putative non-astrocyte cell type markers from the Zhang list that had an expression level >0.25-fold in astrocytes over whole forebrain in the Cahoy list. Genes absent from the Cahoy et al data were excluded. This gave 102 astrocytic genes, 92 neuronal genes, 16 oligodendrocyte precursor cell genes, 26 myelinating oligodendrocyte genes, 33 microglial genes and 30 endothelial genes (Table S1).
***Gene ontology annotation*** was performed using PANTHER version 12 (Mi et al., 2017) using input data as described for Table S5 (genes with >50% change between adult and aged, FPKM of >0.5, expressed at least 0.75-fold of input).
***Cutoffs and comparisons*** Gene lists in supplementary tables were generated as follows.
*Table S3* - all changes in aging: genes with an adjusted p<0.05.
*Table S4* - astrocyte-expressed changes in aging: genes from S3 with an adjusted p<0.05, FPKM >1, expressed at least 0.75-fold of input.
*Table S5* - aging pathway analysis: genes with >50% change between adult and aged, FPKM of >0.5, expressed at least 0.75-fold of input.
*Table S6* – inter-regional comparisons all changes: genes with an adjusted p<0.05.
For intra-cortical comparisons each cortical region was compared to the remaining two cortical regions combined, using batch correction in EdgeR to account for sample non-independence within cortical samples.
For cerebellum and hypothalamus comparisons, CB or HTH were compared against combined cortical samples (MC, SC, VC) using batch correction in EdgeR to account for sample non-independence within cortical samples.
*Table S7* – astrocyte-enriched inter-regional comparisons: genes from S6 with an adjusted p<0.05, FPKM >1, expressed at least 3-fold of input.
*Table S8* - regional pathway analysis: genes with an adjusted p<0.05, FPKM of >1, expressed at least 0.75-fold of input.
***Data presentation*** For gene clustering heatmaps (Figs 2B and 6C), FPKM with a pseudocount of 5 added were used (to decrease the effect of noise of low-expressed genes), and filtered to exclude genes that did not have at least one value >32. These remaining genes (4,401 for aging heatmap, 3,487 for regional comparisons) were log-transformed and clustered using a hierarchical clustering approach: genes were row-scaled and normalized (z-normalized), 1-correlation was used as a distance measure, and the modified Ward's clustering algorithm (part of the R hclust package) was used. Heatmaps were visualized using R version 3.3.2.
Graphs were made with Prism 7 (Graphpad), including scatter plots and heatmaps. InteractiVenn was used to generate Venn diagrams in Figure 2 (Heberle et al., 2015).
Figure 2 - cell-type enrichment, comparing astrocyte-ribotag pulldown to whole brain input. Log2 (fold change) FPKM values averaged from groups of (pulldown FPKM/input FPKM) values from cell-specific genes (Table S1).
Figure 6 - inter-cortical astrocyte comparisons, heatmaps are derived from row z-scores [(ROI FPKM-row mean FPKM)/row standard deviation].
All other heatmaps are based upon log2 (fold change) FPKM values.

**Ribotag characterization: Immunohistochemistry**
***Tissue collection*** 4-month-old astrocyte-ribotag mice were transcardially perfused with 10ml PBS then 10ml chilled 4% PFA, brains extracted, sagittally cut down the midline, and kept 2 hours to overnight in 4% PFA at 4°C, washed with PBS and placed in 30% sucrose at 4°C until brains sank (24-48 hours). Brains were then embedded in tissue freezing medium (General Data Healthcare TFM-5) and flash frozen in dry ice/95% ethanol, then stored at -80°C.
***Sectioning and staining*** Sagittal brain sections were cut on a cryostat (Hacker Industries OTF5000) onto Superfrost Plus slides (Thermo Scientific 4951PLUS4). Brains were sliced at 25µm and dried at 4°C before staining. For immunofluorescent staining, a hydrophobic barrier was drawn around the sections with a paraffin pen, and blocking solution applied onto the slide (5% heat inactivated normal goat serum (NGS), 100 mM L-lysine, 0.2% triton in PBS) and incubated at room temperature for 1 hour. Slides were incubated overnight with primary antibody in 2.5% NGS, 100 mM L-lysine in PBS, then washed 3 x 5 minutes in 0.2% Triton/PBS, then secondary antibody applied at 1:500 dilution (in 2.5% NGS, 100 mM L-lysine, in PBS) and incubated, covered, for 2 hours at room temperature. For experiments with antibodies raised in goat, bovine serum albumin (BSA) was used instead of NGS with 3% BSA in blocking, and 1% in antibody buffers. Slides were then washed 3 x 5 minutes in 0.2% Triton/PBS, and mounted with Slowfade Gold mounting medium with DAPI (ThermoFisher S36939) with 1.5 glass coverslip (ThermoFisher #12544E), sealed with clear nail polish, and dried in the dark for 30 minutes to 1 hour.
***Antibodies*** Astrocyte/ependymal cells: Rb anti-S100b (Abcam ab52642, 1:500 dilution); OPCs: Rb anti-Ng2 (Millipore Ab532,0 1:200); Oligodendrocytes: Ms anti-APC (Calbiochem Op80, 1:50), Microglia: Rb anti-Iba1 (Wako 016-20001, 1:250), Ependymal: Gt anti-Vimentin (Millipore AB1620, 1:150); Neuron: Ms anti-NeuN

(Millipore MAB377, 1:100), Ribotag marker: Rb anti-HA-tag (CST 3724, 1:500); Ribotag marker: Rt anti-HA-tag (Roche 11867423001, 1:100); Rt secondary Ab w/Alexa 488: (Gt anti-Rat IgG, (Molecular Probes A11006, 1:500); Rt secondary Ab w/Alexa 594: (Gt anti-Rat IgG, (Molecular Probes A11007 1:500); Gt secondary Ab w/Alexa 488: (Dk anti-Goat IgG (Molecular Probes A11055 1:500); Ms secondary Ab w/Alexa 488: (Gt anti-Mouse IgG (Molecular Probes A11029 1:500); Ms secondary Ab w/Alexa 594: (Gt anti-Mouse IgG (Molecular Probes A11032 1:500); Rb secondary Ab w/Alexa 488: (Gt anti-Rabbit IgG (Molecular Probes A11034 1:500); Rb secondary Ab w/Alexa 594: (Gt anti-Rabbit IgG (Molecular Probes A11037 1:500); Rb secondary Ab w/Alexa 594: (Dk anti-Rabbit IgG (Molecular Probes A21207 1:500).

***Imaging*** 3 x 16-bit images per brain (from different brain sections – technical replicates), from 3 brains (biological replicates), of 500x500µm of the visual cortex, motor cortex, hypothalamus, and cerebellum were acquired with an AxioImager.Z2 with Apotome.2 module and AxioCam HR3 camera (Zeiss). To image a whole region, multiple tiled images were taken with 10% overlap using the mosaic function, and stitched in Axiovision (Zeiss). A Plan-Apochromatic 20x objective (NA 0.8) was used with 0.37x0.37µm pixel scaling for cell-type specific stains. A Plan-Apochromatic 10x objective (NA 0.45) was used for a whole brain overview of HA stain.

***Analysis*** FIJI (Schindelin et al., 2012) was used to determine the number of ribotag positive cells and their overlap with cell-specific staining. Thresholding was performed on the ribotag labeled image (stained with an anti-HA tag antibody) and the 'Analyze Particles' function was used with a minimum area of 20-40µm to automatically separate and quantify the total number of ribotag positive cells. The number of double-labeled ribotag and cell type antibody positive cells were manually counted. This generated the proportion of ribotag positive cells that also label for the cell-specific marker.

**Ribotag characterization*: qRT-PCR***

To confirm cell-type specificity, RNA from the hypothalamus and cerebellum of 2 year old astrocyte-ribotag pulldowns was compared to RNA isolated from the whole homogenate (input). cDNA was synthesized via rtPCR from 50-100ng of RNA using Superscript VILO master mix (Thermo Fisher Scientific 11755050) according to manufacturer instructions. 2µl of the obtained cDNA was used for qPCR reaction, performed with SYBR green PCR mastermix (ThermoFisher 4309155) (run with a standard protocol on an Applied Biosystems 7300). All samples were run with 3 biological replicates, each consisting of 3 technical replicates. All primers from Integrated DNA Technologies. For analysis, samples were normalized to a housekeeping gene (Gapdh) run in the same qPCR plate with cDNA from the same dilution, and compared to input samples from the same experiment run in the same plate.

Primers used:

Aldhl1l1 (astrocyte, for: CATATTTGCTGACTGCGACCTC; rev: TTCACACCACGTTGGCAATAC);
Gfap (astrocyte, for: TACCAGGAGGCACTTGCTCG; rev: CCACAGTCTTTACCACGATGTTCC);
Syt1 (neuron, for: CTGCATCACAACACTACTAGC; rev: CCAACATTTCTACGAGACACAG);
Psd95 (neuron, for: GTGGGCGGCGAGGATGGTGAA; rev: CCGCCGTTTGCTGGGAATGAA);
Camk2 (neuron, for: AATGGCAGATCGTCCACTTC; rev: ATGAGAGGTGCCCTCAACAC);
Mobp (oligo, for: TCTTCCTCCTGTTCCCTCTCTTG; rev: GGATTTACATTAGGCAAAGCATTGG);
Mbp (oligo, for: GGCAAGGTACCCTGGCTAAA; rev: GTTTTCATCTTGGGTCCGGC);
Gapdh (housekeeping, for: TGCCACTCAGAAGACTGTGG; rev: GCATGTCAGATCCACAATGG)

**GFAP immunohistochemistry**

***Tissue collection*** 2-year-old and 4-month-old C57Bl6/J mice were transcardially perfused with PBS, brains extracted and cut down the midline, embedded in OCT (Scigen #4583), flash-frozen in a 95% ethanol/dry ice bath and kept at -80°C, as outlined above.

***Gfap staining*** 4 x 4-month-old and 4 x 2-year-old brains were sectioned on a cryostat at 20µm (as above), sections stored at -20C, and fixed in 4% PFA for 8 minutes at 4°C, followed by 3 washes in PBS. From there, immunohistochemistry was performed as outlined above with Rb anti-GFAP primary antibody (Abcam ab7260, 1:500 dilution) and Alexa 594-conjugated secondary antibody (Gt anti-Rabbit IgG, Molecular Probes A11037, 1:500).

***Imaging*** 3 x 16-bit tiled images per brain (from different sections – technical replicates), from 4 brains (biological replicates), of hypothalamus and visual cortex per animal were taken of 500µm x 500µm, consisting of 3 x 1.5µm sections in the z-dimension. A Zeiss LSM700 confocal with a Plan-Apochromatic 20x objective (NA 0.8) and AxioObserver camera was used to take images with 0.17x0.17x1.5µm pixel scaling. Identical imaging conditions (laser power, gain) were used for 4-month and 2-year-old samples. The whole brain overview images were acquired using set exposure with an AxioImager.Z2 with a Plan-Apochromatic 10x objective (NA 0.45) and AxioCam HR3 camera (Zeiss) at 0.645x0.645µm pixel scaling.

***GFAP analysis*** For confocal sections, a maximum intensity projection was made from all 3 z-planes, and total fluorescence intensity was quantified using the ImageJ measure function, excluding meninges and pia. Analysis was also performed excluding GFAP around blood vessels, with no difference in outcome.

***In situ* hybridization**

***Tissue collection and processing*** was carried out as described for GFAP staining, and brains were sagittally sectioned at 16-20µm. To perform the *in situs,* RNAscope 2.5 HD multiplex fluorescent Manual Assay kit (ACDbio #320850) was used with modifications - a 25-30 minute permeabilization step using Protease IV (ACDbio #322340) and a final 5 minute DAPI incubation step used to visualize nuclei (1:1000 dilution in PBS; Millipore #5.08741.0001). The primary probe of interest was detected with the Atto-550 detection reagent, with the secondary probe of interest detected using Atto-647 (except for the SPARC experiment, where SPARC was detected with Atto-550, and the secondary probe with Alexa-488).

***Probes*** Serpina3n (Cat #430199 target; NM_009252.2, 745-2005bp); Sparc (#466781-C2; target NM_009242.5, 337-1185bp); Gpc5 (#442831; target NM_175500.4, 389-1414bp); Hspa1b (#488351; target NM_010478.2, 2162-2790bp); C4 (#445161; NM_009780.2, 1644-2631bp); Aldh1l1 (#405891-C2; target NM_027406.1, 1256-2112bp); Aldh1l1 (#405891, target NM_027406.1, 1256-2112); DapB (negative ctrl; #320751, target EF191515, 414-862bp)

***Imaging*** 3 x 16-bit tiled images per region (each from a different brain slice – technical replicates) from 4 brains per age (biological replicates) of at least 500x500µm, with 3 x 1.5µm sections in the z-dimension were obtained. A Zeiss LSM700 confocal with a Plan-Apochromatic 20x objective (NA 0.8) was used to take images with 0.17x0.17x1.5µm pixel scaling. In addition to DAPI, primary probe and secondary probe channels, a blank (unstained) channel was imaged in the 488 wavelength (except for SPARC, whose blank channel was imaged at 647) in order to image auto fluorescent lipofuscin to aid in image analysis (see below). For all experiments, imaging parameters were kept constant between 4-month and 2-year-old samples.

***Analysis*** Analysis of the fluorescent probe signal was hindered in the 2-year old brain due to the high presence of autofluorescent lipofuscin in the aged tissue, which was present in all channels. To eliminate this from the channels containing probe to enable analysis, images were analyzed in Imaris (Bitplane). A 3-dimensional mask from the blank channel (where only lipofuscin fluoresced - see Fig S3) was constructed using the 'surfaces' function using an absolute intensity threshold and size filters. This mask was then subtracted from the channels containing probe, to create an image that just contained signal from the probe. The surface function was then used on this masked channel to define the probe staining area. Total intensity of fluorescence of probe staining, and area of staining, were then quantified with the Imaris 'statistics' function and normalized to tissue volume. Meninges and pia were excluded from analysis. The intensity measure is reported as the ratio of 2-year-old/4-month-old in the figures; the same trends in expression are seen when total area is used for analysis. In order to ensure that the effect seen is not a consequence of altered tissue quality with age, total probe intensity of a given sample was normalized to the total probe intensity of a second *in situ* probe within the same tissue section, Aldh1l1 to mark astrocytes. Second-probe normalized values for a given primary probe exhibit the same trend as non-normalized data.

**Graphs and statistics**

Graphs were made with Prism 7 (Graphpad), including scatter plots and heatmaps. Statistics were performed as outlined in the RNAseq section.

**SUPPLEMENTAL REFERENCES**


Cahoy, J.D., Emery, B., Kaushal, A., Foo, L.C., Zamanian, J.L., Christopherson, K.S., Xing, Y., Lubischer, J.L., Krieg, P.A., Krupenko, S.A., *et al.* (2008). A transcriptome database for astrocytes, neurons, and oligodendrocytes: a new resource for understanding brain development and function. J Neurosci 28, 264-278.

Chai, H., Diaz-Castro, B., Shigetomi, E., Monte, E., Octeau, J.C., Yu, X., Cohn, W., Rajendran, P.S., Vondriska, T.M., Whitelegge, J.P., *et al.* (2017). Neural Circuit-Specialized Astrocytes: Transcriptomic, Proteomic, Morphological, and Functional Evidence. Neuron 95, 531-549.e539.

Doyle, J.P., Dougherty, J.D., Heiman, M., Schmidt, E.F., Stevens, T.R., Ma, G., Bupp, S., Shrestha, P., Shah, R.D., Doughty, M.L., et al. (2008). Application of a Translational Profiling Approach for the Comparative Analysis of CNS Cell Types. Cell 135, 749-762.

Heberle, H., Meirelles, G.V., da Silva, F.R., Telles, G.P., and Minghim, R. (2015). InteractiVenn: a web-based tool for the analysis of sets through Venn diagrams. BMC Bioinformatics 16, 169.

Heiman, M., Kulicke, R., Fenster, R.J., Greengard, P., and Heintz, N. (2014). Cell type–specific mRNA purification by translating ribosome affinity purification (TRAP). Nat Protocols 9, 1282-1291.

Mi, H., Huang, X., Muruganujan, A., Tang, H., Mills, C., Kang, D., and Thomas, P.D. (2017). PANTHER version 11: expanded annotation data from Gene Ontology and Reactome pathways, and data analysis tool enhancements. Nucleic Acids Research 45, D183-D189.

Morel, L., Chiang, M.S.R., Higashimori, H., Shoneye, T., Iyer, L.K., Yelick, J., Tai, A., and Yang, Y. (2017). Molecular and Functional Properties of Regional Astrocytes in the Adult Brain. The Journal of Neuroscience 37, 8706-8717.

Schindelin, J., Arganda-Carreras, I., Frise, E., Kaynig, V., Longair, M., Pietzsch, T., Preibisch, S., Rueden, C., Saalfeld, S., Schmid, B., *et al.* (2012). Fiji: an open-source platform for biological-image analysis. Nat Meth 9, 676-682.

Zhang, Y., Chen, K., Sloan, S.A., Bennett, M.L., Scholze, A.R., O'Keeffe, S., Phatnani, H.P., Guarnieri, P., Caneda, C., Ruderisch, N., *et al.* (2014). An RNA-Sequencing Transcriptome and Splicing Database of Glia, Neurons, and Vascular Cells of the Cerebral Cortex. J Neurosci 34, 11929-11947.